HHS Public Access

Author manuscript

Cell Chem Biol. Author manuscript; available in PMC 2023 September 15.

A genome-wide CRISPR-Cas9 screen identifies CENPJ as a host regulator of altered microtubule organization during *Plasmodium* liver infection

Kamalakannan Vijayan[1,2], **Nadia Arang**[1,3], **Ling Wei**[2], **Robert Morrison**[1,2], **Rechel Geiger**[4], **K. Rachael Parks**[5,6], **Adam J Lewis**[1], **Fred D Mast**[1,2], **Alyse N Douglass**[5], **Heather S Kain**[1,7], **John D Aitchison**[1,2,8,9], **Jarrod S Johnson**[1,10], **Alan Aderem**[1,2,9], **Alexis Kaushansky**[1,2,5,9,11,12,*]

[1] Center for Infectious Disease Research, Seattle, Washington

[2] Seattle Children's Research Institute, Seattle, Washington

[3] current address: University of California, San Diego

[4] MSTP program, University of Washington, Seattle, Washington

[5] Department of Global Health, University of Washington, Seattle, Washington

[6] current address: Fred Hutchinson Cancer Research Center, Seattle, Washington

[7] current address: Bristol Myers Squibb, Seattle, Washington

[8] Department of Biochemistry, University of Washington

[9] Department of Pediatrics, University of Washington

[10] current address: University of Utah, Salt Lake City, Utah

[11]Brotman Baty Institute for precision medicine, Seattle, Washington, Seattle, Washington

[12]Lead contact

Summary

Prior to initiating symptomatic malaria, a single *Plasmodium* sporozoite infects a hepatocyte and develops into thousands of merozoites, in part by scavenging host resources, likely delivered by vesicles. To accomplish this, we showed that host microtubules (MT) dynamically reorganize

* To whom correspondence should be addressed: alexis.kaushansky@seattlechildrens.org.

Author Contributions: K.V., N.A., L.W., R.M., R.G., K.R.P., A.J.L., A.N.D. and H.S.K. performed the experiments. K.V., N.A., L.W., F.D.M., J.D.A., J.S.J., A.A. and A.K. analyzed the data. K.V., L.W. and A.K. wrote the paper with input from all other authors. J.D.A., A.A. and A.K. supervised the research.

Declaration of Interests: The authors declare no competing interests.

Inclusion and Diversity: One or more of the authors of this paper self-identifies as an underrepresented ethnic minority in science. One or more of the authors of this paper received support from a program designed to increase minority representation in science. While citing references scientifically relevant for this work, we also actively worked to promote gender balance in our reference list.

around the developing liver stage (LS) parasite. Using a genome-wide CRISPR-Cas9 screen, we identified host regulators of cytoskeleton organization, vesicle trafficking and ER/Golgi stress regulate LS development. Foci of γ-tubulin localized to the parasite periphery; depletion of Centromere Protein J (CENPJ), a novel regulator identified in the screen, exacerbated this re-localization, and increased infection. We demonstrate that the Golgi acts as a non-centrosomal MT organizing center (ncMTOC) by positioning γ-tubulin and stimulating MT nucleation at parasite periphery. Together, these data support a model where the *Plasmodium* LS recruits host Golgi to form MT mediated conduits along which host organelles are recruited to PVM, and support parasite development.

eTOC blurb

To identify host factors required for *Plasmodium* liver infection, Vijayan et al. conducted a genome wide CRISPR knockout screen in hepatocytes. They demonstrate that liver stage parasites reorganize host microtubules by repositioning the microtubule organizing center at the parasite periphery in a Golgi-dependent fashion.

Graphical Abstract

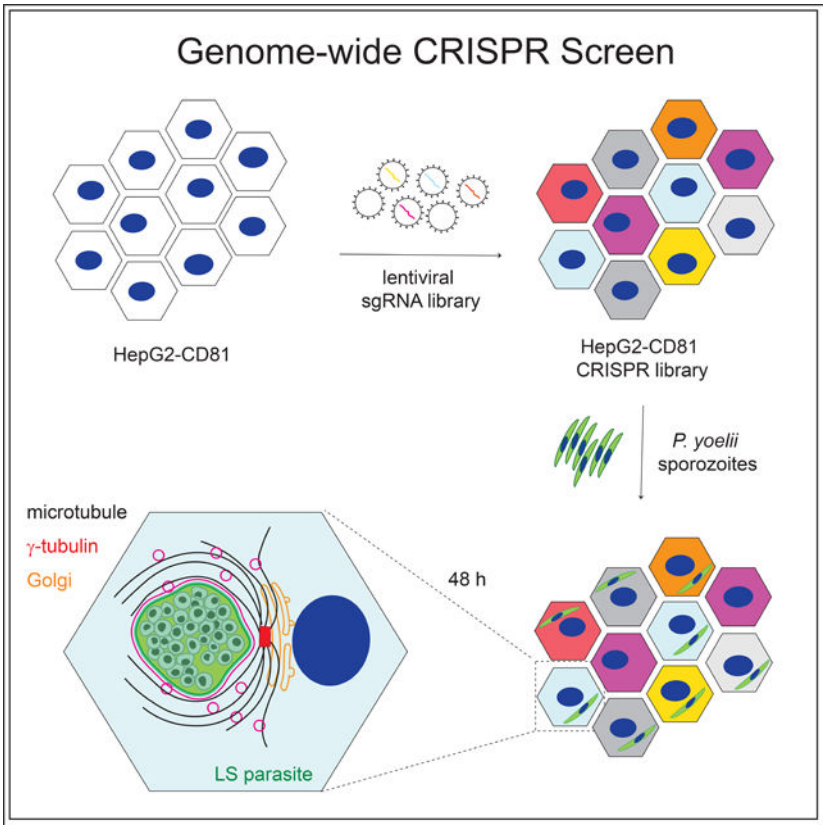

Introduction

Malaria is transmitted to humans by the injection of *Plasmodium* sporozoites into the skin during the blood meal of an infectious female *Anopheles* mosquito. Sporozoites exit

the skin by traversing blood vessels to enter the circulation and are then carried to the liver. Sporozoites leave the circulation by traversing the sinusoidal cell layer, infecting hepatocytes, and subsequently differentiating into LS parasites (Mota et al., 2001; Shortt and Garnham, 1948; Vanderberg, 1981). LS parasites reside in a membrane-bound compartment in the hepatocyte termed the parasitophorous vacuole (PV). Within the PV, LS parasites differentiate into exoerythrocytic merozoites. The PV membrane subsequently breaks down, and merozoites reenter the blood and infect erythrocytes (Sturm et al., 2006).

Hepatocyte infection is obligate for parasite life cycle progression, and thus is an important target for antimalarial intervention. Elimination of the parasite during this stage would block both disease symptoms and transmission. During LS development, host hepatocytes undergo remarkable morphological changes. The cytoskeleton is a key regulator of deformability, and *Plasmodium* has been demonstrated to alter the host cell actin cytoskeleton during LS development (Gomes-Santos et al., 2012), egress (Burda et al., 2017), and blood stage development (Hale et al., 2017; Warncke and Beck, 2019). It has also been shown that the stiffness of hepatocytes is altered during infection, which might also point to an alteration in the host cytoskeleton (Eaton et al., 2012). We and others previously have demonstrated that the *Plasmodium* parasitophorous vacuole membrane (PVM) interacts with late endosomes (Petersen et al., 2017), lysosomes (Lopes da Silva et al., 2012; Niklaus et al., 2019; Prado et al., 2015; Risco-Castillo et al., 2015; Vijayan et al., 2019), retrograde vesicles (Raphemot et al., 2019) and autophagic vesicles (Prado *et al.*, 2015; Real et al., 2018; Wacker et al., 2017). As many intracellular pathogens target the host MT network to subvert host vesicle trafficking events for their own benefit (Alix et al., 2011; Asrat et al., 2014), we hypothesized that *Plasmodium* LS parasites actively alter the host cytoskeleton to traffic the host vesicles to PVM.

Multiple focused forward genetic screens have informed our understanding of host regulatory factors for LS malaria (Prudencio et al., 2008; Raphemot *et al.*, 2019; Rodrigues et al., 2008). These screens have provided valuable insights into parasite-host interactions, but the scope of these investigations have been limited, suggesting that a complete complement of factors required for *Plasmodium* entry and development remains to be discovered. *Plasmodium* LS infection actively remodels the host hepatocyte by rewiring a portion of host cell signaling and disrupting canonical signaling cascades (Glennon et al., 2019). We therefore sought to use an unbiased genome-wide approach to identify the parasite driven host factors that contribute to host cytoskeleton remodeling.

Genome-wide CRISPR screening has emerged as a powerful strategy to identify novel gene functions (Sanjana et al., 2014; Shalem et al., 2014). We report a genome wide CRISPR-Cas9 screen that aims to identify host factors that regulate *Plasmodium* infection. The screen identified several host factors critical for *Plasmodium* development, comprising previously explored and novel host regulators, including those that lead to rearrangement of the cytoskeleton and vesicular trafficking. Our work provides the foundation for a more comprehensive understanding of the host processes that are required for optimal *Plasmodium* development.

Results

P. yoelii-infected cells exhibit alteration in MT organization

To visualize MT organization, we transfected HepG2-CD81 cells with CellLight™ rfp-α-tubulin BacMam 2.0 and infected the cells with *P. yoelii* sporozoites for 6, 24 or 48 h (Fig. 1A). Strikingly, we observed that the host MT network redistributes to the LS parasite, appearing to wrap around the PVM at 24 and 48 hours post infection (h.p.i) but not at 6 h.p.i (Fig. 1A, B, C, S1A and S1B). In contrast, MTs in uninfected cells form a canonical network around the nucleus, radiating toward the cell periphery (Fig. 1A). Acetylated MT are the stabilized form of MT that support kinesin-mediated trafficking of vesicles (Reed et al., 2006). We asked if the MTs associated with the parasite are actively engaged in cell transport by assessing their acetylation status. We infected HepG2-CD81 cells with *P. yoelii* sporozoites for 48 h, and then visualized acetylated α-tubulin and the parasite PVM-resident protein UIS4 by immunostaining (Fig. 1D). MTs that decorate the parasite periphery were highly acetylated. In contrast, in uninfected cells, acetylated MTs were distributed throughout the cytosol (Fig. 1D). We next disassembled the MT by nocodazole treatment (Zhu and Kaverina, 2011). We infected rfp-α-tubulin transfected HepG2-CD81 cells with *P. yoelii* sporozoites. After 46 h, nocodazole was added. After an additional 2h (48h post-infection), cells were washed, and incubated with nocodazole-free media for 45 sec to allow the nucleation of MT (Zhu and Kaverina, 2011). In uninfected cells, MT nucleated close to host nucleus (Fig. 1E). Strikingly, in the infected cells, MTs nucleated adjacent to parasite periphery. Together, these results suggest that during LS development, *P. yoelii* remodels the host MT network to nucleate from the parasite periphery.

CRISPR-Cas9 screen to identify host regulators of infection

Whole genome CRISPR-Cas9 screens facilitate an unbiased approach to identify regulators of a key process (Sanjana et al., 2014; Shalem et al., 2014). To identify host genes critical for MT remodeling during *Plasmodium* LS development, we prioritized breadth in our approach, as canonical regulators of infection are sometimes rewired during infection (Glennon *et al.*, 2019). We used a pooled library of GeCKOv2 sgRNAs to generate a whole-genome knockout library in HepG2-CD81 cells (Sanjana *et al.*, 2014; Shalem *et al.*, 2014). HepG2-CD81 cells were transduced with lentivirus containing the pooled GeCKOv2 sgRNA library of 123,642 sgRNAs targeting 19,031 protein-coding genes (~6 sgRNAs/gene), 1,864 microRNAs (4 sgRNA/microRNA) and 1,000 negative controls (non-targeting sgRNAs that do not recognize any sequence in the genome, 2 sgRNA/control) and selected in puromycin for 5–7 days. To evaluate sgRNA diversity in the HepG2-CD81-GeCKOv2 library, we PCR-amplified the integrated sgRNA cassettes from genomic DNA extracted from transduced cells and subjected the amplified library to Illumina sequencing. At the gene level, 16,629 out of 19,031 (87.38%) genes targeted by 3 or more sgRNAs guides were significantly enriched. We observed an absence of sgRNAs targeting 2402 genes out of 19031 (12.62%); this may be due to gene essentiality or the failure of certain sgRNA to incorporate successfully into the genome. We infected forty million puromycin-resistant cells with green fluorescent protein (GFP) expressing-*Plasmodium yoelii* at a multiplicity of infection (MOI) of 0.3. After 24 h of infection, cells were sorted into infected and bystander cell populations by GFP signal intensity with fluorescence-activated cell sorting (FACS)

(Fig. 2A). Separately, a parallel culture of uninfected cells was also maintained to normalize the sgRNA frequency distributions. We obtained four independent biological replicates with library generation and sequencing occurring in parallel. Genes with significantly enriched sgRNAs were identified for both the bystander and infected populations compared to uninfected cells.

Cells that harbor genetic alterations restricting *P. yoelii* development (i.e., sgRNAs that target host genes important for infection) were expected to be enriched in the uninfected bin; we termed this group 'putative positive regulators of infection'. We categorized sgRNAs enriched in the infected cells as 'putative negative regulators of infection'. In this initial screen, we identified 242 genes that were statistically enriched in infected or bystander groups after accounting for multiple hypotheses. There were 67 genes significantly enriched in the infected cells compared to uninfected cells and 175 genes were significantly enriched in the bystander bin relative to uninfected bin.

To further down-select the high confidence genes, we reasoned that biological pathways with multiple putative regulators were more likely to be bona fide regulators of infection. We performed gene ontology (GO) pathway analysis to identify significantly enriched biological processes (Fig. 2B) using 242 hits from our initial screen. We shortlisted the significant gene regulators present in statistically enriched biological processes for further validation. After this stringent down-selection step, we were left with eight putative negative regulators of infection and seven putative positive regulators of infection for further study (Fig. 2C and D).

Integrating multiple forward genetic screens provides additional testable hypotheses

Here, we report a global screen for host factors that regulate *Plasmodium* LS infection. Yet, like previous focused screens, our screen includes false negatives as sgRNAs are lost during the generation of the library and/or not all sgRNAs result in the disruption of the functional protein. To generate a more comprehensive picture, we systematically compared our screen, which interrogated host regulators of *P. yoelii* infection, with earlier forward genetic screens (Prudencio *et al.*, 2008; Raphemot *et al.*, 2019; Rodrigues *et al.*, 2008) that identified regulators of the closely related parasite, *P. berghei* (Fig. S2A, Supplementary file 1). For the purpose of analysis, we pooled results from the screens by Rodrigues et al., 2008 and Prudencio et al., 2008, as these two screens used the same methodology but had no overlapping factors. To compare our findings to previous screens, we developed a new methodology, meta-analysis by information content (MAIC), to combine data from diverse sources, in the form of ranked gene lists. Briefly, a meta ranking of the three screens was performed by sorting each screen separately by z score, calculating each gene's rank percentile location after sorting, and then averaging the gene rank percentile locations across the three screens, with no penalty for a gene being missing in a screen. This meta ranking was then sorted by average rank percentile location and augmented with the average z score from all screens where the function of the gene was evaluated (Supplementary file 1). Positively and negatively represented genes were sorted separately, then combined afterwards for pathway analysis. At gene level, using the z score cutoff of 2 and 1.5, our screen shared only few hits each of the other screens (Fig. S2B and S2C) without any

common hits across all screens. We reasoned this could be due to many factors including host cell type, parasite species and the methodology employed. When we loosened the stringency of the cutoff to a Z-score of 1, there were several genes overlapping between the three screens, although false positive rates could be higher at this cut-off.

Despite little specific gene overlap, we asked if overlapping pathways and biological processes were present in all the screens. We employed ClueGO to determine gene ontology (GO) (Bindea et al., 2009) and observed significant enrichment in biological processes from the genes represented in at least two of three screens at z-score of 1.5 and 1. Specifically, we identified 18 high confidence biological processes that are significantly enriched using a z-score cutoff of 1.5. This includes biological processes that have been previously described, such as scavenger receptor activity and cholesterol biosynthesis reported (Itoe et al., 2014; Labaied et al., 2011; Petersen *et al.*, 2017; Rodrigues *et al.*, 2008) (Fig. S2D and S2E). Taken together, this combined resource provides a wealth of hypotheses for further investigation.

Identifying host factors that regulate *Plasmodium* LS invasion and development from CRISPR-Cas9 screen

To evaluate the false positive rate of our screen, we individually disrupted each of the 15 putative regulators with three sgRNAs per gene using CRISPR-Cas9 gene editing of HepG2-CD81 cells. In this case we used different sgRNAs against the same 15 regulators identified from the screen to minimize the possibility that our identified hits were the result of an artifact that arose from a specific sgRNA sequence with off-target effects. In this system, a fluorescent reporter, GFP, is expressed only upon guide integration and puromycin resistance, enabling us to exclude any cells that did not take up and integrate the sgRNA (Fig. S3A). GFP positive cells were FACS sorted, cultured with puromycin and the knockout efficiency of 14 genes was further confirmed using western blot (Fig. S3B, S3C and S3D). To identify genes that alter *Plasmodium* LS invasion, we infected each knockout line with *P. yoelii* sporozoites for 90 min and assessed hepatocyte entry by flow cytometry. Among the selected 15 hits, only low-density lipoprotein receptor-related protein 4 (LRP4) exhibited significantly reduced entry of sporozoites 90 min after infection (Fig. 3A). This is consistent with the previous finding that CSP interacts with LRP and HSPG to facilitates host cell invasion of *Plasmodium* (Shakibaei and Frevert, 1996).

As an orthogonal approach, we modulated HepG2-CD81 cells with small molecule inhibitors targeting positive regulators identified in the screen (Fig. 3B) (Supplementary Table 1). IC50 values for each small molecule inhibitor were obtained in uninfected HepG2-CD81 cells using Live/ Dead staining (Fig. S3E). We included eltanexer, an inhibitor of exportin-1 (XPO1), a putative negative regulator of infection (Luedtke et al., 2018; Than et al., 2020). To test the role of LRP4 in sporozoite entry of hepatocytes, we pretreated HepG2-CD81 cells with an LDL-R blocking peptide, which blocks LRP4, and observed a significant decrease in sporozoite entry. Thus, both genetic and peptide-mediated intervention of LRP4 inhibits sporozoite entry of hepatocytes (Fig. 3A and B).

We next performed an imaging-based secondary screen with the selected 15 putative regulators to assess the role of these hits on the parasite burden and longer-term LS

development. This was intended to more closely mirror the experiment performed in the initial screen, although we used a later time point to characterize the full impact on LS development. Specifically, individual CRISPR-Cas9 knockout lines were infected with *P. yoelii* sporozoites and observed 48 h.p.i. Several of the knockout lines exhibited substantially altered LS burden (Fig. 3C). The number of LS parasites was significantly increased in CENPJ (centromere protein J) and KDEL (Lys-Asp-Glu-Leu containing 1) disrupted lines, illustrating that each of these factors is indeed a negative regulator of infection. In contrast, knockout of CISD1 (CDGSH iron sulfur domain 1), COL4A3BP (collagen type IV alpha-3-binding protein), IREB (iron-responsive element-binding protein) and LRP4 significantly reduced the number of LS parasites 48 h.p.i (Fig. 3C). We next tested whether LS infection could be perturbed by targeting these factors with pharmacological inhibitors. Consistent with the genetic experiments, small molecule inhibitors (Supplementary table 1) that target CISD1 (Geldenhuys et al., 2014), COL4A3BP (Santos et al., 2015), IREB (Miyazawa et al., 2019), and LRP4 (Ye et al., 2014), significantly reduced the number of LS parasites observed after 48 h of infection (Fig. 3D), further supporting the notion that these factors are positive regulators of LS infection. Interestingly the UBEK2 inhibitor NSC697923 (Pulvino et al., 2012) significantly reduced the parasite number. We reasoned this might be due to more complete effect of compound than the UBEK2 sgRNA knockout. Alternatively, NSC697923 might also influence other UBEK family proteins, or directly inhibit parasite processes. Similar to its genetic depletion, pharmacological inhibition of FMN2 (Rizvi et al., 2009) and PYGM (Martinez-Navarro et al., 2020) did not alter the parasite numbers.

We next asked if any of the screen hits altered the growth of LS parasites. Knock out of VPS51 (Ang2) and FLNA did not significantly alter parasite load but instead, the size of the parasite was significantly smaller (Fig. 3E). HepG2-CD81 cells expressing sgRNAs directed against COL4A3BP and LRP4 both reduced the number (Fig. 3C) and the size of LS parasites (Fig. 3E). In contrast, depletion of CENPJ and KDEL increased both the size and the number of LS parasites (Fig. 3C, E). Knockout of other putative regulators did not result in altered parasite size (Fig. 3E). Interestingly, while our screen was only set up to identify factors that altered infection rate, not LS growth, it is possible that some slow-growing parasites may have not reached the threshold of GFP levels to be included in the “infected” gate. Together, these studies identified several host factors influencing parasite entry, growth and number (Fig. 3F) and illustrate the utility of genome-scale functional screening for the discovery of host factors that regulate *Plasmodium* LS infection.

γ-tubulin foci sequester at parasite periphery

Among several new regulators of infection identified from the screen, we choose to investigate CENPJ, one of the MT cytoskeleton organizing proteins, in more detail. Depletion of CENPJ resulted in a significant increase in parasite load (Fig. 3C) and growth (Fig. 3E). CENPJ is a conserved, ubiquitously expressed centrosomal protein with a key role in centriole organization and biogenesis (Cho et al., 2006; Ganem et al., 2009; Kohlmaier et al., 2009). The centrosome is a major MT organizing center (MTOC) (Hung et al., 2000). CENPJ depletion impairs centriole assembly, resulting in fragmented MTOCs and a non-radial MT cytoskeleton organization (Cho *et al.*, 2006; Ganem *et al.*, 2009; Kohlmaier

et al., 2009). To characterize the role of CENPJ in parasite development, we assessed the localization of γ-tubulin with γ-TuRC (γ-tubulin ring complex), a core functional unit of the MTOC (Wiese and Zheng, 2000). We infected HepG2-CD81 cells with *P. yoelii* sporozoites and allowed infection to proceed for 48 h. Cells were stained with anti-UIS4 (upregulated in infectious sporozoites gene 4) and γ-tubulin. In uninfected cells, 88% of γ-tubulin foci were localized primarily near nuclear periphery (Fig. 4A). Strikingly, in infected cells, a majority of γ-tubulin foci (~33%) were found in the cytoplasm associated with the parasitophorous vacuolar membrane (PVM) (Fig. 4A and S4).

We evaluated the functional role of CENPJ in regulating the LS parasite. In uninfected, CENPJ-depleted cells, we observed increased cytoplasmic localization (~80%) (Fig. 4A) and multiple γ-tubulin foci (Fig. 4B). Infection in CENPJ knockout cells resulted in an increase in γ-tubulin localization (~66%) to the PVM compared to infected control cells (~33%) (Fig. 4A) and an increase in LS infection (Fig.3C). Infection with LS parasites resulted in MTOC re-localization to the PVM (Fig 4A and B); the absence of CENPJ further exacerbated the non-centrosome MTOC organization close to the PVM that supports LS development (Fig 4A and B).

The host Golgi serves as a non-centrosomal MTOC (ncMTOC) in *P. yoelii* infected cells

Canonically, MT arrays nucleate from MTOCs and radiate towards cell periphery (Wiese and Zheng, 2000). To understand whether the γ-tubulin sequestration resulted in dynamic reorganization of MTs around the parasite, we infected rfp-α-tubulin transfected HepG2-CD81 cells with *P. yoelii* sporozoites, and allowed the infection to proceed for 48 h. After 46 h, nocodazole was added. After an additional 2h (48h post-infection), cells were washed and incubated with nocodazole-free media for 45 sec to allow the nucleation of MTs. Cells were stained with γ-tubulin and UIS4. In uninfected cells, MTs nucleated from γ-tubulin foci at the host nucleus (Fig. 5A). In the infected cells, MTs typically nucleated from γ-tubulin foci localized adjacent to the PVM (Fig. 5A). This suggests that, during infection, MTOCs reorganizes the host MT network around the developing LS parasite.

Several studies have demonstrated that, in the absence of centrosome organizing proteins, Golgi outposts act as a ncMTOCs that function as MT nucleation sites by recruiting γ-tubulin foci ((Grimaldi et al., 2013) reviewed in (Zhu and Kaverina, 2013)). To test whether the parasite localized γ-tubulin foci are regulated by Golgi outposts, we infected rfp-α-tubulin expressing HepG2-CD81 cells with *P. yoelii* sporozoites. As above, nocodazole was added to the cells after 46 hours, and allowed to incubate for two hours. Cells were then washed and incubated for an additional 45 sec to allow MT nucleation. Cells were fixed then stained with antibodies against the Golgi peripheral cytoplasmic membrane protein, Golgi membrane protein of 130 kDa; golgin subfamily A member 2 (GM130), γ-tubulin and UIS4. In uninfected cells, we observed nucleating MTs originating at γ-tubulin foci associated with the host nucleus. In *P. yoelii* infected cells, we primarily observed MTs nucleating from γ-tubulin foci in colocalized with GM130 (Fig. 5B and C) suggesting MTOCs in infected cells are organized at the Golgi.

We next asked if an intact Golgi was required for PVM-associated MTOC formation. To do this, we utilized the small molecules brefeldin A (BFA) or golgicide A (GCA), which disrupt

and fragment the Golgi, blocking assembly and transport of secretory vesicles (Sciaky et al., 1997). We infected rfp-α-tubulin expressing HepG2-CD81 cells with *P. yoelii* sporozoites; after 24h cells were treated with BFA (0.1 μM) or GCA (3.5 μM). Twenty-two hours later (46h post-infection), nocodazole was added to the cells. After an additional 2h (48h post-infection), cells were washed, then incubated with media alone for 45 sec to allow MT nucleation. Cells were stained with antibodies against GM130, γ-tubulin and UIS4. In contrast to infected cells with intact Golgi, following BFA or GCA treatment, γ-tubulin foci failed to re-localize to PVM periphery but instead localized and initiated MT nucleation at the nuclear periphery (Fig. 5B and Fig. S5). Co-localization between Golgi and γ-tubulin foci was substantial in the absence of, but not the presence of, BFA treatment (Fig. 5C). These results are consistent with the hypothesis that Golgi-associated ncMTOCs exist at the parasite periphery and serve to initiate MT reorganization around PVM.

Host Golgi and intracellular vesicles interact with *Plasmodium* LS.

To better understand the role of the Golgi in regulating ncMTOC formation, we investigated the interactions between the Golgi and the PVM during infection. HepG2-CD81 cells were infected with *P. yoelii* sporozoites; after 24h cells were treated with BFA (0.1 μM) or a DMSO control. At 48 h.p.i, cells were stained with antibodies against GM130 and UIS4. We observed UIS4-positive membrane co-localized with Golgi stacks in nearly three quarters of the infected cells at 48 h.p.i (Fig. 6A), consistent with other reports (De Niz et al., 2021; Raphemot *et al.*, 2019). Co-localization between the PVM and Golgi was reduced following BFA treatment (Fig. 6A).

We hypothesized Golgi-mediated MT nucleation at the PVM serves to redirect vesicle traffic to the PVM and facilitate LS survival. This hypothesis is based on two observations: (1) that the Golgi reorients the MTOC to the parasite periphery and (2) that GO terms associated with vesicular trafficking and Golgi and ER stress were significantly enriched as putative regulators of infection in screen (Fig. 2B). We infected HepG2-CD81 cells with *P. yoelii* sporozoites and allowed infection to proceed for 24 or 48 h. Cells were stained with anti-UIS4 and anti-VAMP7 (to visualize intracellular vesicles) to visualize the PVM and host intracellular vesicles, respectively. We observed colocalization between intracellular vesicles and the PVM (Fig. 6B), consistent with other reports (De Niz *et al.*, 2021; Raphemot *et al.*, 2019). The colocalization of intracellular vesicles with the PVM was greatly reduced after BFA treatment (Fig. 6B), suggesting that Golgi integrity (and, likely, subsequent MTOC formation) is important for host vesicle trafficking to PVM. In addition, BFA mediated disruption of association between PVM and host Golgi reduced the parasite load (Fig. 6C) suggesting the importance of the sequestration for LS development. Together, these data suggest the parasite mediates Golgi-associated ncMTOC formation resulting in dynamic reorganization of MTs that redirects vesicular traffic to the PVM, promoting LS development.

Discussion

Plasmodium is auxotrophic and scavenges several metabolites including phosphatidylcholine (Itoe *et al.*, 2014), lipoic acid (Deschermeier et al., 2012) and cholesterol (Labaied *et al.*,

2011) from the host. Multiple screening efforts and other reports (Lopes da Silva *et al.*, 2012; Petersen *et al.*, 2017; Prudencio *et al.*, 2008; Raphemot *et al.*, 2019; Real *et al.*, 2018; Rodrigues *et al.*, 2008; Vijayan *et al.*, 2019) have pointed to the critical role of vesicular transport throughout *Plasmodium* LS infection. Vesicle mediated trafficking is the well-established route of intracellular lipid trafficking and it is enticing to speculate, a tool that the *Plasmodium* exploits for nutrient acquisition. While the host organelle decoration of the PVM is a well-documented phenomenon, perturbating any particular subclass of vesicles does not completely abrogate the parasite growth. This suggests that the parasite does not have an absolute requirement for any specific vesicle that has been tested to date. Instead, our data suggest that the LS parasite usurps nearly all vesicular traffic by reorienting the MTOC.

To identify the host genes involved in the active MT remodeling, we performed genome-wide CRISPR knockout screen in HepG2-CD81 cells. Previous forward-genetic screens have identified host factors involved in *Plasmodium* infection (Prudencio et al., 2008; Raphemot et al., 2019; Rodrigues et al., 2008). These screens have exhibited very little overlap in identified factors, presumably in part because each screen prioritized identifying a small, but bona fide list of “hits,” and suffered a high false negative rate as a result. These efforts have led to many key discoveries into interactions between the malaria parasite and its host hepatocyte but have fallen short of providing a truly comprehensive picture of all regulators of infection. Like the earlier screens, the CRISPR-Cas9 screen we report here does not exhibit substantial overlap with previous screens when individual gene hits are evaluated, suggesting that additional analysis is still needed to comprehensively assess factors that regulate infection. Yet, when we evaluate whether hits from our screen are present in similar pathways to those observed in other screens, the overlap is substantial. Thus, while we may have, as a field, identified many central regulatory biological functions that control LS development, we have yet to saturate our understanding of the molecular players that mediate these biological necessities. Together, the CRISPR-Cas9 screen we present here, along with the previously reported siRNA screens, represent a key resource for the field moving forward, and we anticipate that merging findings from these experiments will provide many additional hypotheses to probe. The analysis of the screen, performed to date, has limitations. Since it is likely that at least a subset of canonical signaling pathways are rewired in the course of infection (Glennon et al., 2019), pathway analysis, which is based primarily on canonical signaling networks, is unlikely to comprehensively and accurately describe the topology of the signaling relationships that mediate the complex host-parasite interface. Developing tools to reconstruct signaling relationships, within the context of malaria infection, is a critical area for future investigation.

The proximity between Golgi and PVM suggests that the Golgi could act as a ncMTOCs to remodel MT network. Here we show that when Golgi is disrupted with inhibitors BFA or GCA the association between MTOC and PVM is lost (Figure 5B), along with subsequent vesicular traffic to PVM (Figure 6B). Thus, parasite control of host MTs may occur primarily via docking of host MTOC to the PVM by direct interactions between the PVM and the Golgi. Future work could define the specific role of relocalizing the MTOC in LS infected hepatocytes. Some possibilities include: (i) facilitating the accumulation of phospholipids needed for membrane growth or (ii) developing a stable structure around the

PVM to provide mechanical support to PVM. Similar reorganization of the host MT network to facilitate the hijacking of host vesicles has been reported in *Toxoplasma gondii* (Coppens et al., 2006), suggesting that this may be a conserved mechanism by which apicomplexan parasites facilitate nutrient uptake and survival.

Our work describes a global regulatory mechanism by which host materials contained within vesicles is carried to the PVM; it leaves the question of how vesicles engage, or even fuse with the PVM for future study. Multiple studies have suggested that host factors are present at the PVM or even further within the parasite compartment (Itoe *et al.*, 2014; Labaied *et al.*, 2011; Lopez-Perez et al., 2006; Niklaus *et al.*, 2019; Petersen *et al.*, 2017; Raphemot *et al.*, 2019; Real *et al.*, 2018), so it is tempting to speculate that vesicle contents are delivered to the parasite through vesicle-PVM fusion. The fusion of vesicles with other membranous compartments (organelles, plasma membrane) is well studied (reviewed in (Jackson et al., 2016)); future work could investigate if similar mechanisms facilitate the delivery of cargo to the parasite or whether parasite proteins exported to the PVM, mediate engagement with host vesicles. A more comprehensive molecular understanding of how the parasite acquires nutrients and other materials from the host cell could facilitate our capacity to intervene against the rapidly growing LS parasite.

Significance

New strategies to combat malaria in the field are desperately needed. The causative agent of malaria, the obligate intracellular parasite *Plasmodium*, relies heavily on its mammalian host to survive and develop. A better understanding of how the parasite scavenges host factors for nutrition and/or reorganizes host components for its own survival is needed. Here we show that the liver stage parasite actively remodels host MT network. Using a genome wide forward genetic screen, we demonstrate a mechanism by which the parasite remodels the host cytoskeleton to redirect host vesicular traffic to the parasite and facilitate its development. Our work implicates diverse host processes in LS *Plasmodium* development, which may inspire subsequent work in the field and/or may be leveraged to develop pharmacological agents to fight malaria.

Limitations of the study

In this study, we observe altered MT behavior in *Plasmodium*-infected hepatocytes that results in host vesicular traffic being redirected to the PVM. Although we systematically explored this process using temporally resolved immunofluorescence imaging, our work does not describe in detail the timing of this remodeling event. Subsequent work that utilizes live cell imaging could add temporal detail to our findings.

The functional studies contained within this manuscript are performed using pharmacological inhibitors and CRISPR knock outs, each which have off-target effects. For example, in our study, pharmacological inhibition of COL4A3BP resulted in decreased sporozoite invasion at 90 mins whereas genetic depletion did not influence the sporozoite invasion. There exist multiple possibilities for these seemingly disconnected data points. First, either the small molecule (HPA-12) or the genetic knockdown of COL4A3BP could have resulted in off-target effects that drive the phenotype. Alternatively, the longer

timeframe of the CRISPR knockout experiment could have led to compensatory effects that produced the phenotype. Finally, the different time scales of the blocking the molecule in the two experiments could have altered the impact on infection. Each of these possibilities will need to be systematically evaluated in future studies.

In our CRISPR/Cas9 screen, cells were infected by P. yoelii at an MOI of 0.3., which leads to a large population of cells being uninfected due to the lack of chance to encounter the parasites. To partially overcome this, we isolated infected and uninfected cells by FACS. Yet, using this small population of cells in the infected pool and large number of bystander cells left uninfected due to low MOI used, may have introduced noise, complicating the analysis.

All the 15 genes we chose to validate had only one guide that gave a significant phenotype in the screen (Supplemental file 5). This could be due to the combination of use of high stringency in shortlisting the genes and low signal to noise ratio of the screen. Validation was performed with a set of sgRNA (3 sgRNAs / gene) independent of the ones used in the screen (Figure 3). Alternative approaches to down-select hits for further study would have produced different genes for follow-up. We have provided raw data from the screen (Supplemental file 2, 3 and 4) and are hopeful readers will use it to inspire investigation into additional biological regulators of the Plasmodium liver stage parasite.

STAR Methods

Resource Availability

Lead Contact—Further information and requests for resources and reagents should be directed to and will be fulfilled by the Lead Contact, Alexis Kaushansky (alexis.kaushansky@seattlechildrens.org).

Materials Availability—All unique reagents generated in this study are available from the Lead Contact with a completed Materials Transfer Agreement.

Data and Code Availability—All data reported in this paper will be shared by the lead contact upon request. Any additional information required to reanalyze the data reported in this paper is available from the lead contact upon request. This paper does not report original code.

Experimental Model and Subject Details

Cell lines and cell culture—HepG2-CD81 cells (Silvie et al., 2006) were modified from HepG2 hepatoma cells isolated from a hepatocellular carcinoma of a 15-year-old, Caucasian, male (ATCC, USA). Cells were maintained in DMEM-Complete Medium (Dulbecco's modified eagle medium (Cellgro, Manassas, VA), supplemented with 10% v/v FBS (Sigma-Aldrich, St. Louis, MO), 10000 IU/ml penicillin, 100 mg/ml streptomycin (Cellgro), 2.5 mg/ml fungizone (HyClone/Thermo Fisher, Waltham, MA) and 4 mM L-Glutamine (Cellgro). Cells were split 2–3 times weekly.

Mosquito rearing and sporozoite production—For *P. yoelii* sporozoite production, female 6–8-week-old Swiss Webster mice (Harlan, Indianapolis, IN) were injected with

blood stage *P. yoelii* (17XNL) parasites to begin the growth cycle. Animal handling was conducted according to the Institutional Animal Care and Use Committee-approved protocols. Briefly, *Anopheles stephensi* mosquitoes were allowed to feed on infected mice after gametocyte exflagellation was observed. Salivary gland sporozoites were isolated using a standard protocol at day 14 or 15 post-blood meal. The sporozoites were activated with 20% v/v FBS and pelleted by centrifugation at 1,000 × *g* to salivary gland detritus. Sporozoites were further enriched by a second centrifugation at 15,000 × *g* for 4 min at 4 °C, before resuspension in a desired volume of complete medium.

Method Details

Pooled genome-wide CRISPR screen—To perform the whole-genome CRISPR screen, HepG2-CD81 cells were transduced with lentivirus containing the GeCKOv2 pooled sgRNA library of 123,642 sgRNAs targeting 19,031 protein-coding genes (~6 sgRNAs/gene), 1,864 microRNAs (4 sgRNA/microRNA) and 1,000 negative controls (2 sgRNA/control), and selected in puromycin for 5–7 days. On day 12–14 post-transduction, 40 million puromycin-resistant cells were infected with GFP tagged-*P. yoelii* at a MOI of 0.3. After 24 h of infection, cells were sorted as infected and uninfected by FACS into different bins based on GFP signal. A non-treated, non-infected control was also collected for each experiment to assess library representation. The experiment was performed four independent times. Genomic DNA from each sample was isolated using QIAamp DNA mini kit (Qiagen, Hilden, Germany).

Next-generation sequencing—Libraries were generated using a 2-step PCR according to previously published protocol (Sanjana *et al.*, 2014). Briefly, an initial PCR was performed using AccuPrime Pfx Supermix (Invitrogen, Waltham, MA, USA) with lentiCRISPRv2 adaptor primers to amplify the sgRNA region and add priming sites for Illumina indexing. Amplicons were purified using FlashGels (Lonza, Allendale, NJ, USA) and purified PCR products were used as templates for subsequent PCR amplification. Sufficient PCR reactions were performed to maintain library coverage. Next, a second PCR was performed in order to add Illumina P5 and P7 index sequences, as well as barcodes for multiplexing, and samples were re-purified. Purified libraries were quantified using the KAPA library quantification kit (Kapa Biosystems, Wilmington, MA, USA) as per manufacturer's instructions performed on an Applied Biosystems 7500 Fast real-time PCR machine (Applied Biosystems, Foster City, CA, USA). Samples were sequenced on a MiSeq (Illumina) using the manufacturer's protocol with addition of Illumina PhiX control (Illumina, San Diego, CA, USA) to improve library diversity at a final concentration of 10% per library volume. After demultiplexing, FASTQ data files of 75bp single mate reads averaged 24.98 million raw reads per library.

Differential abundance of guides and gene enrichment analysis—FASTQ files were aligned to the GeCKOv2 pooled sgRNA library of 123, 642 sgRNA DNA sequences by Bowtie2 (version 2.2.8) using local alignment policy command line arguments " --local -L 12 -N 0 -D 15 -i C,1,0 --gbar 8 --rdg 10,3 --rfg 10,3". This yielded on average 20.41 million aligned reads to guides per library. Read counts per guide were converted to relative expression abundance as Reads Per Million (RPM). A guide was called detected in a screen

if the before infection condition was at least 0.1 RPM. Undetected guides (RPM below 0.1) were excluded from further calculations. 16,629 out of 19,031 (87.38%) genes targeted by 3 or more guides/ sgRNA were detected in least 3 experiments. Fold change with respect to 'before infection' was calculated by dividing RPM in 'infected' or 'bystanders' conditions by RPM in 'before infection' condition. The differential abundance of a guide is represented as the $\log_2$ ratio of fold change in 'infected' condition divided by the fold change in 'bystanders' condition. If less than two screens call a guide detected (RPM >= 0.2), a $\log_2$FC of 0 and p-value of 1 are reported for this guide. Otherwise, the final $\log_2$FC of the guide is the arithmetic mean of the $\log_2$ ratios from each detected screen, and the final p-value of the guide is calculated by one sample t-test that the $\log_2$ ratios of the detected guides was not zero. The GeCKO library contains 6 independent guides for each protein-coding gene. The $\log_2$FC and p-value at the gene level is calculated from $\log_2$FC and p-value of its 6 guides. The $\log_2$FC of a gene is equal to the $\log_2$FC of the guide with the lowest (best) p-value. The corrected p-value of a guide is set to 1 if the sign of its $\log_2$FC is opposite to the $\log_2$FC of the gene. Then the p-value of a gene is calculated as the product of corrected p-values from all guides not excluded from calculations. Thus, genes with multiple guides that alter infection in the same direction are more likely to be ranked highly using the corrected p-value metric.

Gene set enrichment analysis on all genes with positive/negative $\log_2$FC was performed based on major knowledgebases including HUGO Gene Nomenclature Committee (HGNC), Gene Ontology (GO), Kyoto Encyclopedia of Genes and Genomes (KEGG) and Reactome. The top 200 significantly enriched gene sets associated with all genes of negative or positive $\log_2$FC were identified. Genes that are both statistically significant (p-value < 0.05) and differentially abundant ($\log_2$FC < −6.0 or > 6.0) were considered significantly represented in *P. yoelii* infection. Go terms were clustered into higher order hierarchy using ClueGO plug-in (version 2.3.3), implemented in Cytoscape v3.4.0.

Generation of individual hits using gene specific CRISPR sgRNA—GFP tagged vectors for the 15 hits were obtained from ABM Good (Richmond, British Columbia, Canada). Non-replicating lentiviral stocks were generated by transfection of HEK293-FT cells. 4×10^6 HEK293-FT cells were plated on poly-L-lysine coated dishes to achieve 70–80% confluency at time of transfection. Approximately 24 h after plating, transfection mixtures were prepared by mixing 20 μl Polyethyleneimine MAX (Polysciences Inc, Warrington, PA) prepared at 1 mg/ml, together with 4.75 μg of sgRNA construct or a scramble control, along with 3rd generation lentiviral packaging mix from ABM Good, according to manufacturer's protocol. After incubating for 10 min at room temp in DMEM, transfection complexes were added dropwise to cells. After overnight incubation, cells were washed to remove transfection mixtures and were fed with 10 ml fresh media. Lentivirus-containing supernatant was harvested 36 hours later, passed through 0.45 μm syringe filters, and either used immediately for transduction or stored at −80 °C. To disrupt candidate genes, HepG2-CD81 cells were transduced with lentiviral supernatants in 6-well plates at a cell density of 1×10^6 per well. At time of plating, cells were transduced with 1 ml of supernatant in the presence of 0.5 μg/ml polybrene (Sigma Aldrich St. Louis, MO). In order to select for cells with stable integration of shRNA transgenes, supernatant was replaced

with complete media with the addition of 2 μg/ml puromycin 24 h post-transduction, and cells were selected for at least 5 days prior to experiments. For analysis of experiments with the knockout cells, only the GFP-positive cells have been considered.

Western blot—5×10^5 HepG2-CD81 scramble and knockout cells were seeded in each well of a 24-well plate (Corning). Cells were briefly washed with ice-cold PBS and then scraped into a Triton X-100-based lysis buffer (1% Triton X-100, 10 mM beta-glycerol phosphate, 10 mM pyrophosphate, 40 mM HEPES pH 7.4, 2.5 mM MgCl2 with 1 tablet of ethylenediaminetraacetic acid (EDTA)-free protease inhibitor per 50 mL buffer). Cell lysates were clarified by centrifugation at 17,000 × g at 4 °C for 10 min. Lysed cells were denatured with SDS at 95°C for 5 minutes and separated on an 10% SDS PAGE at 200 V for 30 minutes. iBlot2—Fast Protein Transfer System ThermoScientific, United States) was used for blotting, and proteins were stained using the antibodies specified. The details of the antibodies were included in the star methods section. Proteins were visualized using Chemidoc imaging system (Bio-Rad laboratories, United States). Western blot band intensities were measured using ImageJ. Average pixel intensities were collected over equal area boxes for bands. Pixel densities were then inverted by subtracting 255 from all values. Background controls were then subtracted from corresponding band intensities and normalized with β-actin loading control.

Infection assay—5×10^5 HepG2-CD81 wild type cells or knockout cells were seeded in each well of a 24-well plate (Corning) and infected with *P. yoelii* sporozoites at an MOI of 0.3 for 90 min and the infection was either stopped, or media was replaced and the infection was allowed to progress for 48 h. For drug treatment experiments, cells were either pretreated for 24 h and washed before infection or post treated following 24 h of infection as mentioned and the infection was allowed to proceed for 48 h.

Flow cytometry to assess sporozoite invasion—5×10^5 HepG2-CD81 wild type cells or knockdown cells were seeded in each well of a 24-well plate (Corning) and infected with *P. yoelii* sporozoites at an MOI of 0.3 for 90 min. Cells were detached with accutase (Life technologies) and fixed with Cytoperm/Cytofix (BD Biosciences). Cells were blocked with Perm/Wash (BD Biosciences) + 2% (w/v) BSA for one hour at room temperature then stained overnight at 4 °C with Alexa Fluor −488 or −647 conjugated circumsporozoite (CSP) antibody. The cells were then washed and resuspended in PBS supplemented with 5 mM EDTA. Infection rates were measured by flow cytometry on an LSRII (Becton-Dickinson) and analyzed with FlowJo (Tree Star).

Immunofluorescence—For imaging experiments, HepG2-CD81 wild type or knockout cells were plated in 8 well chamber slides (Labtek) and infected with *P. yoelii* sporozoites. Cells were fixed with 3.7% (v/v) paraformaldehyde (Sigma) at defined timepoints after infection (90 min, 24 h or 48 h), permeabilized with Triton X-100, and stained with fluorescent tagged UIS-4 or other antibodies mentioned. Nuclei were stained with DAPI (Vectashield). Images were acquired with a 100× 1.4 NA objective (Olympus) on a DeltaVision Elite High-Resolution Microscope (GE Healthcare Life Sciences). The sides of each pixel represent 64.5 × 64.5 nm and z-stacks were acquired at 300 nm intervals.

Approximately 20–30 slices were acquired per image stack. For deconvolution, the 3D data sets were processed to remove noise and reassign blur by an iterative Classic Maximum Likelihood Estimation widefield algorithm provided by Huygens Professional Software (Scientific Volume Imaging BV, The Netherlands). Images for processed with IMARIS Bitplane, image analysis software to quantify LS, perform colocalization analysis and remove outlier cells. For the high throughput secondary screen, cells were plated onto 96 well plate, infected and stained as explained above. Images were acquired using Keyence BZ-X800 automated microscope and infection rate were quantified using Imaris 9.5, image analysis software.

Image analysis and quantification—3D reconstruction of z-stack images was performed with IMARIS (Bitplane). Deconvolved images of immuno-stained cells with anti-UIS4 (PVM), α-tubulin (MTs), γ-tubulin (MTOCs), DAPI (nucleus) were processed, thresholded and segmented by Imaris software to render isosurfaces or isospots.

MTs and the PVM/nuclear association: A 3μm extended area around PVM and nucleus isosurfaces were masked. Total intensity of MT within the masked area around PVM and nucleus was measured and normalized over the area of the nucleus and PVM, respectively. Fold change in normalized MT intensity around PVM to host nucleus was calculated. MT intensity fold change of 2 or above is considered as positive association.

MTOC and PVM association: In control cells, we observed the distance between mTOC and nucleus ranges from 0–3 μm. Since the mTOC is canonically associated with the nucleus, we set this as the value of an “associated” mTOC. Thus, we used 3 μm as a threshold distance to score the mTOC association either with host nucleus or PVM.

MTOC and MT association: Isosurfaces for MT and isospots for MTOC structures were created with IMARIS using 3-D reconstructed z-stack images. MTOC isospots within 0.5μm from the MT isosurface were considered as association.

Golgi and VAMP7 association with PVM and MTOC: We used the coloc tool directly on the respective channels to analyze the Pearson’s colocalization coefficient.

LS parasite size measurement: UIS-4 staining of PVM was utilized to generate isosurface for LS parasite in IMARIS and the surface area of the LS forms were calculated using area measurement tool.

MT nucleation assay—For analysis of Golgi nucleation of MT, cells were treated with 20 nM nocodazole for 2 h at 37 °C and immediately incubated with extraction buffer (60 mM PIPES, 25 mM HEPES, 10mM EGTA, 2 mM MgCl2, 0.1% Tritón X-100, pH 6.9, supplement with 0.25 nM nocodazole and 0.25 nM taxol) for 45 s. Cells were then fixed with methanol and stained with antibody anti GM130 and antibody anti α-tubulin. For BFA treatment experiments, HepG2-CD81-rfp-tubulin cells were infected with *P. yoelii* sporozoites for 48 h; after 24h, cells were treated with BFA. 22 h after BFA treatment, cells were treated with 20 nM nocodazole for 2 h at 37 °C and immediately incubated with extraction buffer (60 mM PIPES, 25 mM HEPES, 10mM EGTA, 2 mM MgCl2, 0.1%

Tritón X-100, pH 6.9, supplement with 0.25 nM nocodazole and 0.25 nM taxol) for 45 s. Cells were then fixed with methanol and stained with antibody mentioned. Images were acquired with a 100× 1.4 NA objective (Olympus) on a DeltaVision Elite High-Resolution Microscope (GE Healthcare Life Sciences) and analyzed as explained above.

Meta-analysis of screens—Z-scores of positively and negatively represented genes in each screen were calculated separately. Meta ranking was performed by function metaRank() from the R package DuffyTools, (using arguments: mmode="percentile", rank.average. FUN=mean, naDropPercent = 0.75). Positively represented genes with z-scores greater than the cutoff (1.0, 1.5, 2.0) and negatively represented genes with z-scores smaller than the cutoff (−1.0, −1.5, −2.0) were selected as hits for each screen. Hits of positively and negatively represented genes were combined for further pathway enrichment analysis. To compare datasets of uneven sizes, gene rank percentiles were assigned to positively and negatively represented genes in each screen separately. Genes were ranked by the average percentiles across all datasets where they were screened.

Gene Ontology analysis on integrated forward genetic screens—Identified hit genes from all the four screens were uploaded in all possible combinations in the ClueGO plug-in (version 2.3.3), implemented in Cytoscape v3.4.0 (http://cytoscape.org/) to generate gene ontology (GO) and pathway enrichment networks. Enriched functionally annotated groups were obtained with the following setting parameters: organism was set to Homo sapiens; the total gene set used in each of the screen were used as reference; the gene ontology terms were accessed from the following ontologies/pathways: Biological Process and Reactome Pathway database evidence code was restricted to 'All_without_IEA'. The GO fusion option was also selected. The significance of each term was calculated with a two-sided hypergeometric test corrected with Benjamini-Hochberg correction for multiple testing. The kappa score was set to 0.5 and the GO tree levels were restricted at 6–16 (medium-detailed specificity). For GO term selection, a minimum of 3 genes and 3% coverage of the gene population was set. GO terms were grouped with an initial group size of 2 and 50% for group merge. The remaining parameters were set to defaults.

Quantification and Statistical analysis—Statistical significance was determined with a one-way ANOVA with multiple comparisons or two-tailed unpaired student t-test. Analyses were performed using GraphPad Prism version 8 for Windows. Statistical tests used, what n represents, and precision measures can be found in figure legends.

Supplementary Material

Refer to Web version on PubMed Central for supplementary material.

Acknowledgements:

This research was funded by National Institutes of Health grants R01GM101183 (AK), R00AI111785 (AK), a W.M. Keck Foundation award (AK), U19AI100627 (AA) R01AI032972 (AA), U19AI111276 (JDA), and P41GM109824 (JDA). We thank the Seattle Children's Research Institute vivarium staff for their work with mice and insectary staff for their work with mosquitoes. Human GeCKOv2 CRISPR knockout pooled library was a gift from Feng Zhang.

References

Alix E, Mukherjee S, and Roy CR (2011). Subversion of membrane transport pathways by vacuolar pathogens. The Journal of cell biology 195, 943–952. 10.1083/jcb.201105019. [PubMed: 22123831]

Asrat S, de Jesus DA, Hempstead AD, Ramabhadran V, and Isberg RR (2014). Bacterial pathogen manipulation of host membrane trafficking. Annu Rev Cell Dev Biol 30, 79–109. 10.1146/annurev-cellbio-100913-013439. [PubMed: 25103867]

Bindea G, Mlecnik B, Hackl H, Charoentong P, Tosolini M, Kirilovsky A, Fridman WH, Pages F, Trajanoski Z, and Galon J (2009). ClueGO: a Cytoscape plug-in to decipher functionally grouped gene ontology and pathway annotation networks. Bioinformatics 25, 1091–1093. 10.1093/bioinformatics/btp101. [PubMed: 19237447]

Burda PC, Caldelari R, and Heussler VT (2017). Manipulation of the Host Cell Membrane during Plasmodium Liver Stage Egress. mBio 8. 10.1128/mBio.00139-17.

Cho JH, Chang CJ, Chen CY, and Tang TK (2006). Depletion of CPAP by RNAi disrupts centrosome integrity and induces multipolar spindles. Biochem. Biophys. Res. Commun. 339, 742–747. 10.1016/j.bbrc.2005.11.074. [PubMed: 16316625]

De Niz M, Caldelari R, Kaiser G, Zuber B, Heo WD, Heussler VT, and Agop-Nersesian C (2021). Hijacking of the host cell Golgi by Plasmodium berghei liver stage parasites. J. Cell Sci. 134. 10.1242/jcs.252213.

Deschermeier C, Hecht LS, Bach F, Rutzel K, Stanway RR, Nagel A, Seeber F, and Heussler VT (2012). Mitochondrial lipoic acid scavenging is essential for Plasmodium berghei liver stage development. Cell Microbiol 14, 416–430. 10.1111/j.1462-5822.2011.01729.×. [PubMed: 22128915]

Eaton P, Zuzarte-Luis V, Mota MM, Santos NC, and Prudencio M (2012). Infection by Plasmodium changes shape and stiffness of hepatic cells. Nanomedicine 8, 17–19. 10.1016/j.nano.2011.10.004.

Ganem NJ, Godinho SA, and Pellman D (2009). A mechanism linking extra centrosomes to chromosomal instability. Nature 460, 278–282. 10.1038/nature08136. [PubMed: 19506557]

Geldenhuys WJ, Leeper TC, and Carroll RT (2014). mitoNEET as a novel drug target for mitochondrial dysfunction. Drug Discov Today 19, 1601–1606. 10.1016/j.drudis.2014.05.001. [PubMed: 24814435]

Glennon EKK, Austin LS, Arang N, Kain HS, Mast FD, Vijayan K, Aitchison JD, Kappe SHI, and Kaushansky A (2019). Alterations in Phosphorylation of Hepatocyte Ribosomal Protein S6 Control Plasmodium Liver Stage Infection. Cell Rep 26, 3391–3399 e3394. 10.1016/j.celrep.2019.02.085. [PubMed: 30893610]

Gomes-Santos CS, Itoe MA, Afonso C, Henriques R, Gardner R, Sepulveda N, Simoes PD, Raquel H, Almeida AP, Moita LF, et al. (2012). Highly dynamic host actin reorganization around developing Plasmodium inside hepatocytes. PLoS One 7, e29408. 10.1371/journal.pone.0029408. [PubMed: 22238609]

Grimaldi AD, Fomicheva M, and Kaverina I (2013). Ice recovery assay for detection of Golgi-derived microtubules. Methods Cell Biol. 118, 401–415. 10.1016/B978-0-12-417164-0.00024-0. [PubMed: 24295320]

Hale VL, Watermeyer JM, Hackett F, Vizcay-Barrena G, van Ooij C, Thomas JA, Spink MC, Harkiolaki M, Duke E, Fleck RA, et al. (2017). Parasitophorous vacuole poration precedes its rupture and rapid host erythrocyte cytoskeleton collapse in Plasmodium falciparum egress. Proc. Natl. Acad. Sci. U. S. A. 114, 3439–3444. 10.1073/pnas.1619441114. [PubMed: 28292906]

Hung LY, Tang CJ, and Tang TK (2000). Protein 4.1 R-135 interacts with a novel centrosomal protein (CPAP) which is associated with the gamma-tubulin complex. Mol Cell Biol 20, 7813–7825. 10.1128/mcb.20.20.7813-7825.2000. [PubMed: 11003675]

Itoe MA, Sampaio JL, Cabal GG, Real E, Zuzarte-Luis V, March S, Bhatia SN, Frischknecht F, Thiele C, Shevchenko A, and Mota MM (2014). Host cell phosphatidylcholine is a key mediator of malaria parasite survival during liver stage infection. Cell Host Microbe 16, 778–786. 10.1016/j.chom.2014.11.006. [PubMed: 25498345]

Jackson CL, Walch L, and Verbavatz JM (2016). Lipids and Their Trafficking: An Integral Part of Cellular Organization. Dev. Cell 39, 139–153. 10.1016/j.devcel.2016.09.030. [PubMed: 27780039]

Kohlmaier G, Loncarek J, Meng X, McEwen BF, Mogensen MM, Spektor A, Dynlacht BD, Khodjakov A, and Gonczy P (2009). Overly long centrioles and defective cell division upon excess of the SAS-4-related protein CPAP. Curr. Biol. 19, 1012–1018. 10.1016/j.cub.2009.05.018. [PubMed: 19481460]

Labaied M, Jayabalasingham B, Bano N, Cha SJ, Sandoval J, Guan G, and Coppens I (2011). Plasmodium salvages cholesterol internalized by LDL and synthesized de novo in the liver. Cell. Microbiol. 13, 569–586. 10.1111/j.1462-5822.2010.01555.×. [PubMed: 21105984]

Lopes da Silva M, Thieleke-Matos C, Cabrita-Santos L, Ramalho JS, Wavre-Shapton ST, Futter CE, Barral DC, and Seabra MC (2012). The host endocytic pathway is essential for Plasmodium berghei late liver stage development. Traffic (Copenhagen, Denmark) 13, 1351–1363. 10.1111/j.1600-0854.2012.01398.×.

Lopez-Perez IC, Risco-Castillo V, Collantes-Fernandez E, and Ortega-Mora LM (2006). Comparative effect of Neospora caninum infection in BALB/c mice at three different gestation periods. The Journal of parasitology 92, 1286–1291. 10.1645/GE-883R.1. [PubMed: 17304808]

Luedtke DA, Su Y, Liu S, Edwards H, Wang Y, Lin H, Taub JW, and Ge Y (2018). Inhibition of XPO1 enhances cell death induced by ABT-199 in acute myeloid leukaemia via Mcl-1. J Cell Mol Med 22, 6099–6111. 10.1111/jcmm.13886. [PubMed: 30596398]

Martinez-Navarro FJ, Martinez-Morcillo FJ, Lopez-Munoz A, Pardo-Sanchez I, Martinez-Menchon T, Corbalan-Velez R, Cayuela ML, Perez-Oliva AB, Garcia-Moreno D, and Mulero V (2020). The vitamin B6-regulated enzymes PYGL and G6PD fuel NADPH oxidases to promote skin inflammation. Dev Comp Immunol 108, 103666. 10.1016/j.dci.2020.103666. [PubMed: 32126244]

Miyazawa M, Bogdan AR, and Tsuji Y (2019). Perturbation of Iron Metabolism by Cisplatin through Inhibition of Iron Regulatory Protein 2. Cell Chem Biol 26, 85–97 e84. 10.1016/j.chembiol.2018.10.009. [PubMed: 30449675]

Mota MM, Pradel G, Vanderberg JP, Hafalla JC, Frevert U, Nussenzweig RS, Nussenzweig V, and Rodriguez A (2001). Migration of Plasmodium sporozoites through cells before infection. Science 291, 141–144. 10.1126/science.291.5501.141. [PubMed: 11141568]

Niklaus L, Agop-Nersesian C, Schmuckli-Maurer J, Wacker R, Grunig V, and Heussler VT (2019). Deciphering host lysosome-mediated elimination of Plasmodium berghei liver stage parasites. Scientific reports 9, 7967. 10.1038/s41598-019-44449-z. [PubMed: 31138850]

Petersen W, Stenzel W, Silvie O, Blanz J, Saftig P, Matuschewski K, and Ingmundson A (2017). Sequestration of cholesterol within the host late endocytic pathway restricts liver-stage Plasmodium development. Molecular biology of the cell 28, 726–735. 10.1091/mbc.E16-07-0531. [PubMed: 28122820]

Prado M, Eickel N, De Niz M, Heitmann A, Agop-Nersesian C, Wacker R, Schmuckli-Maurer J, Caldelari R, Janse CJ, Khan SM, et al. (2015). Long-term live imaging reveals cytosolic immune responses of host hepatocytes against Plasmodium infection and parasite escape mechanisms. Autophagy 11, 1561–1579. 10.1080/15548627.2015.1067361. [PubMed: 26208778]

Prudencio M, Rodrigues CD, Hannus M, Martin C, Real E, Goncalves LA, Carret C, Dorkin R, Rohl I, Jahn-Hoffmann K, et al. (2008). Kinome-wide RNAi screen implicates at least 5 host hepatocyte kinases in Plasmodium sporozoite infection. PLoS Pathog 4, e1000201. 10.1371/journal.ppat.1000201. [PubMed: 18989463]

Pulvino M, Liang Y, Oleksyn D, DeRan M, Van Pelt E, Shapiro J, Sanz I, Chen L, and Zhao J (2012). Inhibition of proliferation and survival of diffuse large B-cell lymphoma cells by a small-molecule inhibitor of the ubiquitin-conjugating enzyme Ubc13-Uev1A. Blood 120, 1668–1677. 10.1182/blood-2012-02-406074. [PubMed: 22791293]

Raphemot R, Toro-Moreno M, Lu KY, Posfai D, and Derbyshire ER (2019). Discovery of Druggable Host Factors Critical to Plasmodium Liver-Stage Infection. Cell Chem Biol 26, 1253–1262 e1255. 10.1016/j.chembiol.2019.05.011. [PubMed: 31257182]

Real E, Rodrigues L, Cabal GG, Enguita FJ, Mancio-Silva L, Mello-Vieira J, Beatty W, Vera IM, Zuzarte-Luis V, Figueira TN, et al. (2018). Plasmodium UIS3 sequesters host LC3 to avoid elimination by autophagy in hepatocytes. Nat Microbiol 3, 17–25. 10.1038/s41564-017-0054-×. [PubMed: 29109477]

Reed NA, Cai D, Blasius TL, Jih GT, Meyhofer E, Gaertig J, and Verhey KJ (2006). Microtubule acetylation promotes kinesin-1 binding and transport. Curr Biol 16, 2166–2172. 10.1016/j.cub.2006.09.014. [PubMed: 17084703]

Risco-Castillo V, Topcu S, Marinach C, Manzoni G, Bigorgne AE, Briquet S, Baudin X, Lebrun M, Dubremetz JF, and Silvie O (2015). Malaria Sporozoites Traverse Host Cells within Transient Vacuoles. Cell host & microbe 18, 593–603. 10.1016/j.chom.2015.10.006. [PubMed: 26607162]

Rizvi SA, Neidt EM, Cui J, Feiger Z, Skau CT, Gardel ML, Kozmin SA, and Kovar DR (2009). Identification and characterization of a small molecule inhibitor of formin-mediated actin assembly. Chem Biol 16, 1158–1168. 10.1016/j.chembiol.2009.10.006. [PubMed: 19942139]

Rodrigues CD, Hannus M, Prudencio M, Martin C, Goncalves LA, Portugal S, Epiphanio S, Akinc A, Hadwiger P, Jahn-Hofmann K, et al. (2008). Host scavenger receptor SR-BI plays a dual role in the establishment of malaria parasite liver infection. Cell host & microbe 4, 271–282. 10.1016/j.chom.2008.07.012. [PubMed: 18779053]

Sanjana NE, Shalem O, and Zhang F (2014). Improved vectors and genome-wide libraries for CRISPR screening. Nat Methods 11, 783–784. 10.1038/nmeth.3047. [PubMed: 25075903]

Santos C, Fleury L, Rodriguez F, Markus J, Berkes D, Daich A, Ausseil F, Baudoin-Dehoux C, Ballereau S, and Genisson Y (2015). The CERT antagonist HPA-12: first practical synthesis and individual binding evaluation of the four stereoisomers. Bioorg Med Chem 23, 2004–2009. 10.1016/j.bmc.2015.03.019. [PubMed: 25818765]

Sciaky N, Presley J, Smith C, Zaal KJ, Cole N, Moreira JE, Terasaki M, Siggia E, and Lippincott-Schwartz J (1997). Golgi tubule traffic and the effects of brefeldin A visualized in living cells. J Cell Biol 139, 1137–1155. 10.1083/jcb.139.5.1137. [PubMed: 9382862]

Shakibaei M, and Frevert U (1996). Dual interaction of the malaria circumsporozoite protein with the low density lipoprotein receptor-related protein (LRP) and heparan sulfate proteoglycans. J Exp Med 184, 1699–1711. 10.1084/jem.184.5.1699. [PubMed: 8920859]

Shalem O, Sanjana NE, Hartenian E, Shi X, Scott DA, Mikkelson T, Heckl D, Ebert BL, Root DE, Doench JG, and Zhang F (2014). Genome-scale CRISPR-Cas9 knockout screening in human cells. Science 343, 84–87. 10.1126/science.1247005. [PubMed: 24336571]

Shortt HE, and Garnham PC (1948). The pre-erythrocytic development of Plasmodium cynomolgi and Plasmodium vivax. Trans R Soc Trop Med Hyg 41, 785–795. 10.1016/s0035-9203(48)80006-4. [PubMed: 18865442]

Silvie O, Greco C, Franetich JF, Dubart-Kupperschmitt A, Hannoun L, van Gemert GJ, Sauerwein RW, Levy S, Boucheix C, Rubinstein E, and Mazier D (2006). Expression of human CD81 differently affects host cell susceptibility to malaria sporozoites depending on the Plasmodium species. Cellular microbiology 8, 1134–1146. 10.1111/j.1462-5822.2006.00697.×. [PubMed: 16819966]

Sturm A, Amino R, van de Sand C, Regen T, Retzlaff S, Rennenberg A, Krueger A, Pollok JM, Menard R, and Heussler VT (2006). Manipulation of host hepatocytes by the malaria parasite for delivery into liver sinusoids. Science 313, 1287–1290. 10.1126/science.1129720. [PubMed: 16888102]

Than H, Pomicter AD, Yan D, Beaver LP, Eiring AM, Heaton WL, Senina A, Clair PM, Shacham S, Mason CC, et al. (2020). Coordinated inhibition of nuclear export and Bcr-Abl1 selectively targets chronic myeloid leukemia stem cells. Leukemia. 10.1038/s41375-020-0708-1.

Vanderberg JP (1981). Plasmodium berghei exoerythrocytic forms develop only in the liver. Trans R Soc Trop Med Hyg 75, 904–905. 10.1016/0035-9203(81)90445-4. [PubMed: 7036442]

Vijayan K, Cestari I, Mast FD, Glennon EKK, McDermott SM, Kain HS, Brokaw AM, Aitchison JD, Stuart K, and Kaushansky A (2019). Plasmodium Secretion Induces Hepatocyte Lysosome Exocytosis and Promotes Parasite Entry. iScience 21, 603–611. 10.1016/j.isci.2019.10.054. [PubMed: 31731198]

Wacker R, Eickel N, Schmuckli-Maurer J, Annoura T, Niklaus L, Khan SM, Guan JL, and Heussler VT (2017). LC3-association with the parasitophorous vacuole membrane of Plasmodium berghei liver stages follows a noncanonical autophagy pathway. Cellular microbiology 19. 10.1111/cmi.12754.

Warncke JD, and Beck HP (2019). Host Cytoskeleton Remodeling throughout the Blood Stages of Plasmodium falciparum. Microbiol. Mol. Biol. Rev. 83. 10.1128/MMBR.00013-19.

Wiese C, and Zheng Y (2000). A new function for the gamma-tubulin ring complex as a microtubule minus-end cap. Nat Cell Biol 2, 358–364. 10.1038/35014051. [PubMed: 10854327]

Ye H, Zhao Q, Huang Y, Wang L, Liu H, Wang C, Dai D, Xu L, Ye M, and Duan S (2014). Meta-analysis of low density lipoprotein receptor (LDLR) rs2228671 polymorphism and coronary heart disease. Biomed Res Int 2014, 564940. 10.1155/2014/564940. [PubMed: 24900971]

Zhu X, and Kaverina I (2011). Quantification of asymmetric microtubule nucleation at subcellular structures. Methods Mol. Biol. 777, 235–244. 10.1007/978-1-61779-252-6_17.

Zhu X, and Kaverina I (2013). Golgi as an MTOC: making microtubules for its own good. Histochem Cell Biol 140, 361–367. 10.1007/s00418-013-1119-4. [PubMed: 23821162]

Highlights:

- A genome wide CRISPR screen identifies host factors of *Plasmodium* liver infection.
- *Plasmodium* liver stages reorganize the host microtubule (MT) network.
- Host Golgi acts as non-centrosomal MT organizing complex (MTOC) at parasite periphery.
- Golgi mediated MTOC repositioning regulates host vesicular trafficking to the parasite.

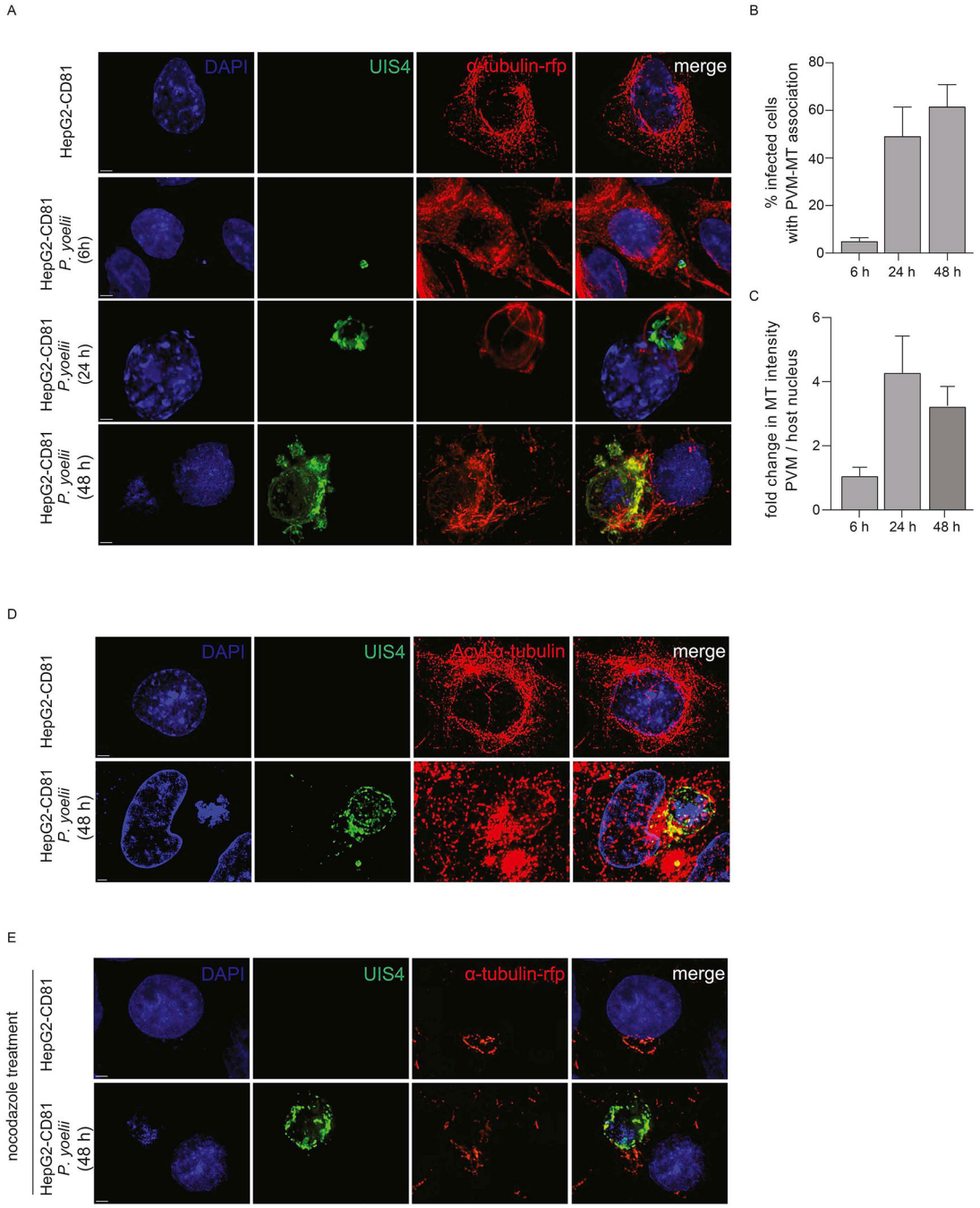

Figure 1. *P. yoelii*-infected cells exhibit alterations in MT organization.

(A) HepG2-CD81 cells transfected with CellLight™ rfp-α-tubulin BacMam 2.0 were infected with *P. yoelii* sporozoites for 6, 24 or 48 h. Cells were fixed and stained with antibodies to UIS4. Images are maximum intensity projections of 20–25 z-slices from a representative positive association. **(B)** The bar graph represents parasitophorous vacuole membrane (PVM) and MT association. Images and the bar graph are a representative of from 3 independent experiments with n ≥ 100 cells / condition. **(C)** The bar graph represents fold change in MT intensity in the masked ROI around PVM and host nucleus. The bar

graph is a representative of 3 independent experiments with n ≥ 25 cells / condition. **(D)** HepG2-CD81 cells were infected with *P. yoelii* sporozoites for 48 h, fixed and stained with antibodies to *P. yoelii* UIS4 and acetylated α-tubulin. Images are maximum intensity projections from 20–25 z-slices. **(E)** HepG2-CD81 cells were infected with *P. yoelii* sporozoites for 48 h. Nocodazole (2.5 nM) was added to the cells after 46h for 2 hours. Cells were washed and incubated for 45 sec to allow the nucleation of MT. Cells were fixed and stained with antibodies to UIS4–647 conjugate. Images and bar graph are a representative of 3 independent experiments with n ≥ 100 cells / condition. Bar = 2 μm. See also Figure S1.

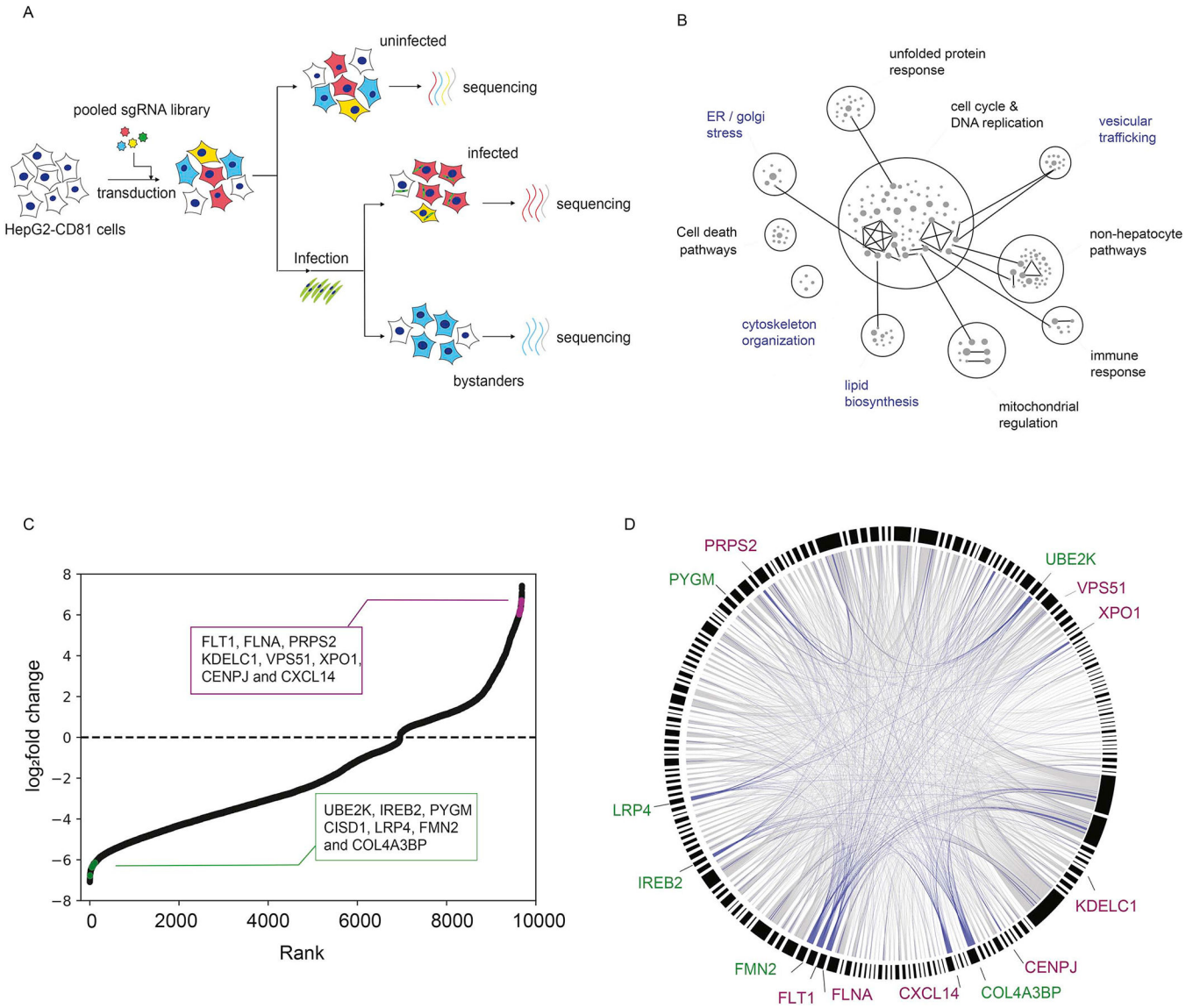

Figure 2. Whole genome hepatoma CRISPR-Cas9 screen reveals putative *Plasmodium* liver stage regulatory factors.

(A) Workflow of the hepatoma CRISPR-Cas9 screen. A pooled CRISPR-Cas9 lentiviral sgRNA library is used to transduce HepG2-CD81 cells. Cells are infected with GFP-expressing *P. yoelli* sporozoites, and infected cells are isolated via FACS. Four biological samples were collected, and Illumina sequenced to quantify sgRNA counts from: uninfected cells, infected cells, and bystander cells. **(B)** sgRNAs observed at different levels in infected and uninfected cells are enriched in multiple GO biological processes. Nodes represent different biological processes, and the size of each node is scaled to the number of sgRNAs in the underlying gene set. Connection between nodes indicates that they share at least one gene. The nodes are grouped and further annotated. The nodes highlighted in blue are highly represented and characterized further in the study. GO terms are clustered based on higher order hierarchy using ClueGo cytoscape plugin. **(C)** Ranked $\log_2$ FC of genes with different levels of sgRNAs in infected and uninfected cells with a p-value < 0.05. Genes selected

for further study are colored magenta (log_2 FC > 0; negative regulators of infection) or green (log_2FC < 0; positive regulators of infection). **(D)** A chord diagram of genes with significantly enriched sgRNAs in infected vs uninfected cells (p-value < 0.05, log_2FC < −6.0 or > 6.0). An edge connecting genes indicates that they both belong to at least one gene set according to GO terms. Genes selected for further study are colored magenta (log_2 fold change>0) or green (log_2FC <0). Blue coded edges represent the connection between the genes belonging to the GO terms highlighted in **(B)**. See also Figure S2 and Table S2.

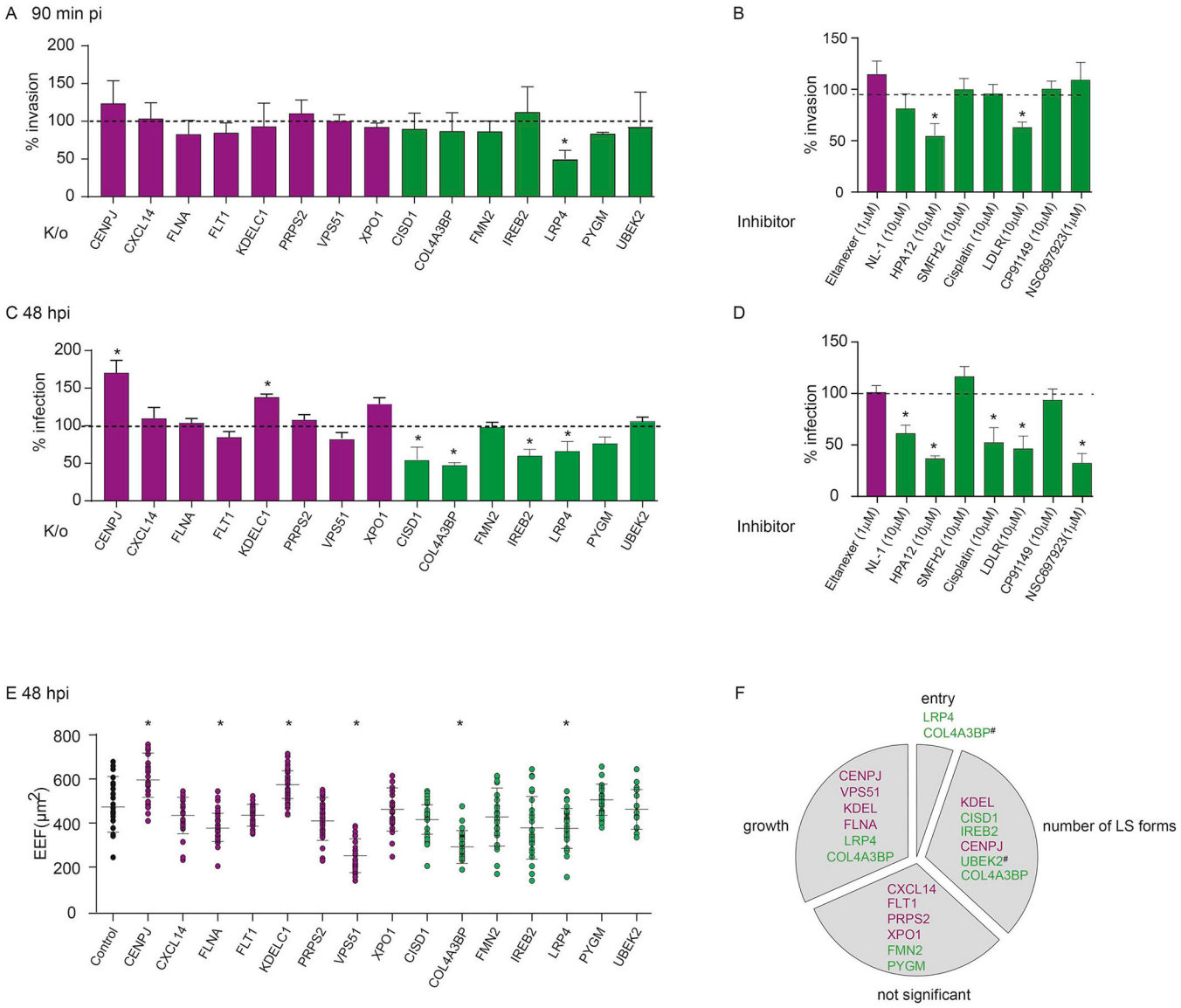

Figure 3. Evaluation of selected hits from CRISPR-Cas9 screen for activity in LS infection and development.

(A) HepG2-CD81 cells were transfected with CRISPR-Cas9 containing plasmids targeting the specified gene or scrambled control and challenged with *P. yoelii* sporozoites for 90 min. The bar graph depicts invasion as the rate of *Py*CSP-positive cells for each sgRNA knockout, normalized to a scrambled control. Magenta represents negative regulators of infection and green represents positive regulators of infection. Data represents mean values ± SE from three independent experiments. * denotes $p<0.05$ and the p values were determined by comparing each knockout to scramble control using one-way ANOVA for multiple comparisons test. **(B)** HepG2-CD81 cells were pre-treated with or without the presence of specified compounds for 2 h and infected with *P. yoelii* sporozoites for 90 min. As in **(A)**, the bar graph depicts the invasion rate. Data represents mean values ± SE from three independent experiments. * denotes $p<0.05$ and the p values were determined by comparing each treatment to control using one-way ANOVA for multiple comparisons test.

(C) HepG2-CD81 cells were transfected with CRISPR-Cas9 containing plasmids targeting the specified gene or scrambled control and challenged with *P. yoelii* sporozoites. After 48 h, infection was evaluated using fluorescence microscopy. The bar graph depicts the infection rate after knockout of each transcript of interest normalized to scramble cells. Data represents mean values ± SE from three independent experiments. * denotes $p<0.05$ and the p values were determined by comparing each knockout to scramble control using one-way ANOVA for multiple comparisons test. **(D)** HepG2-CD81 cells were infected with *P. yoelii* sporozoites for 90 min, washed and treated with or without the presence of specified compounds for 48 h. As in **(C)** the bar graph depicts the infection rate. Data represents mean values ± SE from three independent experiments. * denotes $p<0.05$ and the p values were determined by comparing each treatment to control using one-way ANOVA for multiple comparisons test. **(E)** Assessment the liver stage (LS) parasite size from **(C)**. Data represents mean values ± SE of 20 LS forms from three independent experiments. * denotes $p<0.05$ and the p values were determined by comparing each treatment to control using one-way ANOVA for multiple comparisons test. **(F)** A pie chart depicts knockout or inhibitor treatment of specific genes that led to altered parasite invasion (as in part **A**, **B**), number of parasite (as in part **C**, **D**) or growth (part **E**). Genes are marked with # if inhibitors to the protein, but not sgRNA to the gene, altered the phenotype (e.g., UBEK2, COL4A3BP). See also Figure S3 and Table S1.

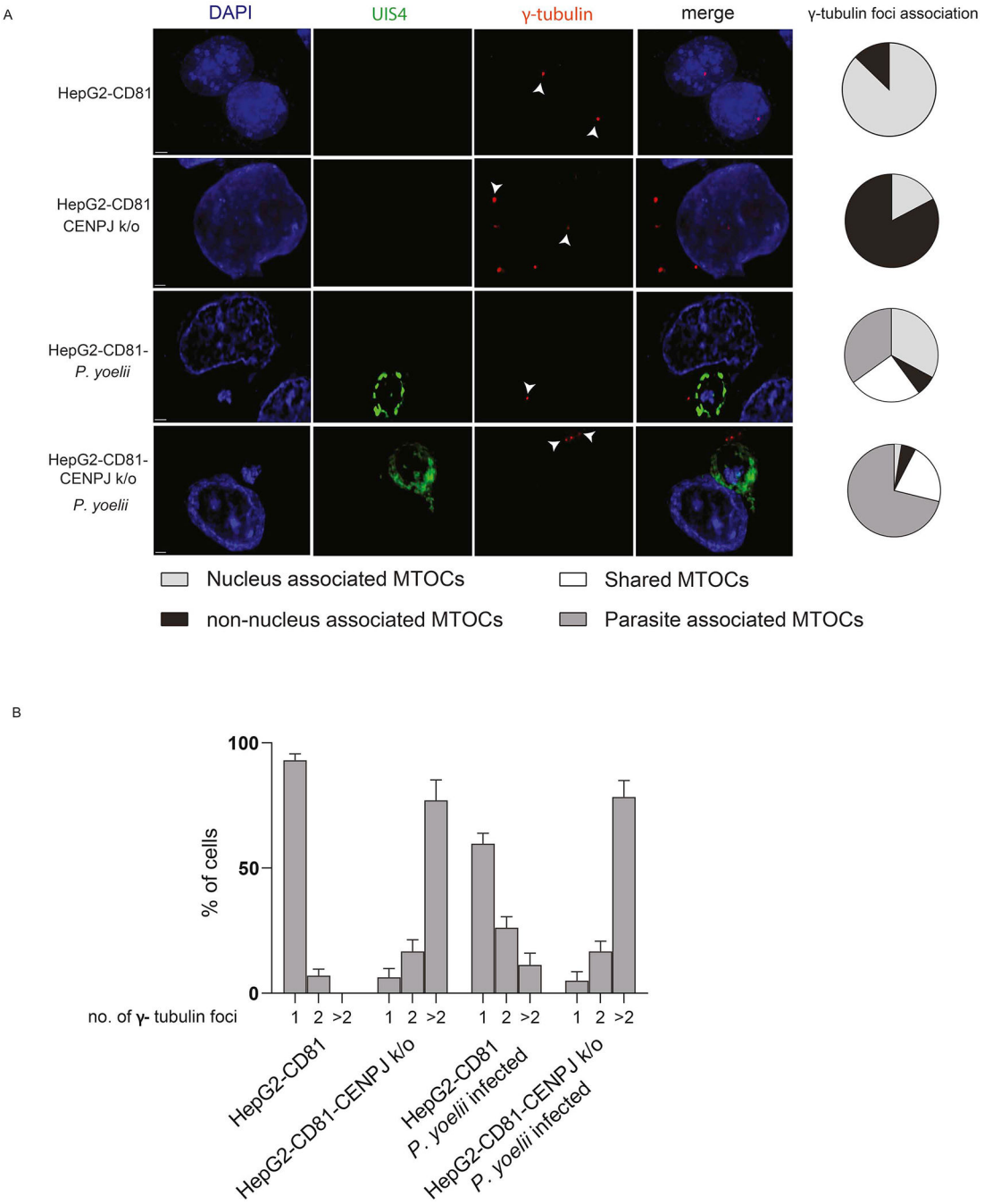

Figure 4. γ-tubulin foci sequester at parasite periphery.

(A) HepG2-CD81-scramble control and HepG2-CD81-sgRNA-CENPJ cells were infected with *P. yoelii* sporozoites for 48 h. Cells were fixed and stained with antibodies against UIS4-Alexa 647 conjugate (pseudo-colored green) and γ-tubulin to visualize the parasite PVM and the γ-tubulin foci, respectively. White arrow heads points to γ-tubulin foci. A pie chart showing localization of γ-tubulin in the cell during different conditions. Images are maximum intensity projections from 20–25 z-slices. Images are a representative of 3 independent experiments with n ≥ 100 cells / condition. Bar = 2 μm **(B)** A bar graph

representing percentage of cells containing multiple γ-tubulin foci. Data represents mean values ± SE from three independent experiments: with n ≥ 100 infected cells. * denotes $p<0.05$ and the p values were determined by comparing each condition to scramble control using one-way ANOVA for multiple comparisons test. See also Figure S4.

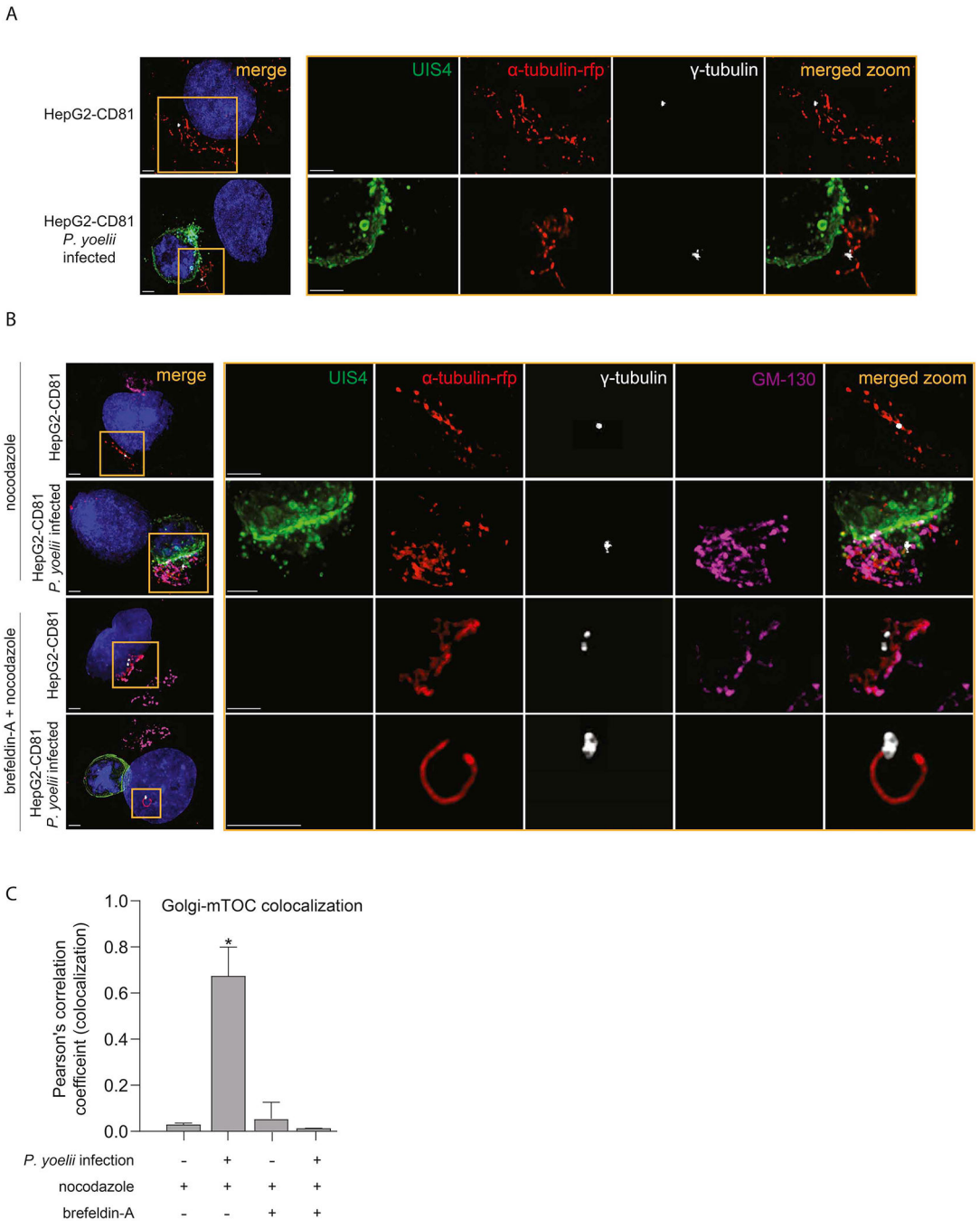

Figure 5. Golgi acts as ncMTOC in *P. yoelii* infected cells.

(A) HepG2-CD81-rfp-tubulin cells were infected with *P. yoelii* sporozoites for 48 h. After 46 h, nocodazole (2.5 nM) was added. After an additional 2h (48h post-infection), cells were washed, and incubated for 45 sec to allow the nucleation of MT. Cells were stained with UIS4 and γ-tubulin to visualize the parasite PVM and the MTOC, respectively. **(B)** HepG2-CD81-rfp-tubulin cells were infected with *P. yoelii* sporozoites; after 24h, cells were treated with BFA (0.1 μM). After an additional 22 hours (46h post-infection), nocodazole (2.5 nM) was added to the cells for 2 h, cells were washed, then incubated with media alone

for 45 sec to allow MT nucleation. Cells were fixed and stained with antibodies against GM130, UIS4 and γ-tubulin to visualize Golgi, parasite PVM and the MTOCs, respectively. Images are representative of 3 independent experiments with n ≥ 100 infected and control cells. Bar = 2 μm. **(C)** Intensity based colocalization was performed between GM-130 (Golgi) and γ-tubulin (MTOCs) on at least 100 cells per condition from **(B)** and Pearson's correlation coefficients were calculated. The bar graph represents Pearson's correlation coefficient calculated from **(B).** Data represents mean values ± SE from three independent experiments: with n ≥ 100 infected cells. * denotes $p<0.05$ and the p values were determined by comparing each condition to no treatment control using one-way ANOVA for multiple comparisons test. See also Figure S5.

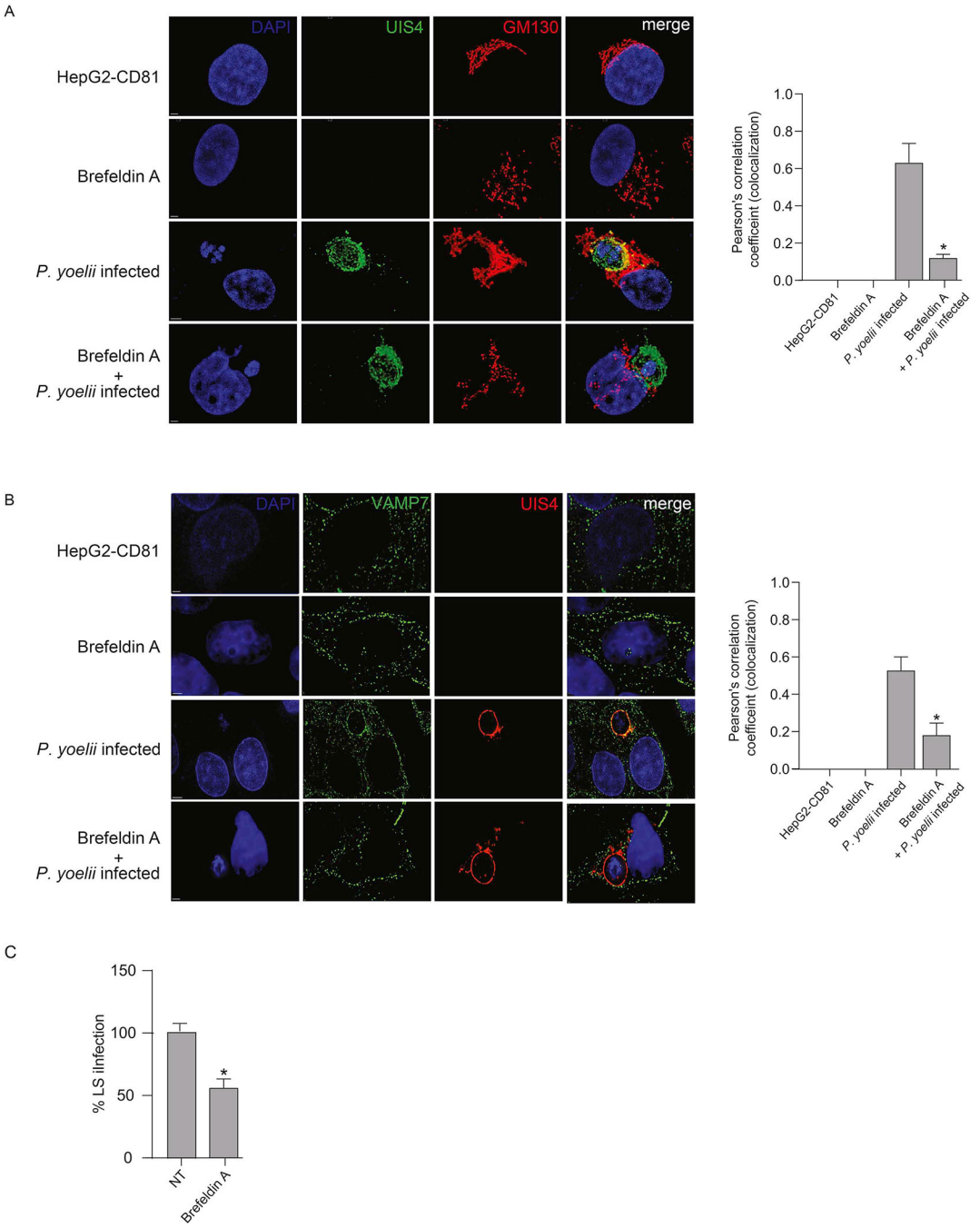

Figure 6. Host Golgi and intracellular vesicles interacts with *Plasmodium*.

(A) HepG2-CD81 cells were infected with *P. yoelii* sporozoites for 48 h. Cells were treated with BFA (0.1 μM) following 24 h of infection. Cells were fixed and stained with Golgi GM130 and UIS4 to visualize host Golgi and the parasite PVM, respectively. A representative maximum intensity projection of is shown. **(B)** HepG2-CD81 cells were infected with *P. yoelii* sporozoites for 48 h. Cells were treated with BFA (0.1 μM) following 24 h of infection. Cells were fixed and stained with VAMP7 and UIS4 to visualize host intracellular vesicles and the parasite PVM, respectively. A representative maximum

intensity projection of is shown for **(A)** and a single z-image is shown for **(B)**. Images in **(A)** and **(B)** are representative of 3 independent experiments with n ≥ 100 infected and control cells. Bar = 2 μm. Intensity based colocalization was performed on at least 100 cells per condition and Pearson's correlation coefficients were calculated. Data represents mean values ± SE from three independent experiments. * denotes $p<0.05$ and the p values were determined by comparing each condition to no treatment control using one-way ANOVA for multiple comparisons test. **(C)** The bar graph depicts the infection rate quantified from **(A)**. Data represents mean values ± SE from three independent experiments. * denotes $p<0.05$ and the p values were determined by comparing each condition to no treatment control using student t-test.

Key resources table

REAGENT or RESOURCE	SOURCE	IDENTIFIER
Antibodies		
Anti-UIS4	LifeSpan BioScience, Inc.	Cat# LS-C204260, RRID: AB_2333159
Anti-CENPJ	Proteintech	Cat# 11517-1-AP, RRID: AB_2244605
Anti-CXCL14	Abcam	Cat# ab129183, RRID: AB_11141827
Anti-FLNA	Cell Signaling Technology	Cat# 4762S, RRID: AB_2106408
Anti-FLT1	Cell Signaling Technology	Cat# 2893, RRID:AB_2106857
Anti-KDELC1	Thermo Fisher Scientific	Cat# PA5-71415, RRID:AB_2690829
Anti-PRPS2	Santa Cruz Biotechnology	Cat# sc-134425, RRID:AB_2171532
Anti-VPS51	Thermo Fisher Scientific	Cat# PA5-21674, RRID:AB_11156373
Anti-XPO1	Cell Signaling Technology	Cat# 46249, RRID:AB_2799298
Anti-CISD1	Cell Signaling Technology	Cat# 83775, RRID:AB_2800031
Anti-COL4A3BP	Abcam	Cat# ab72536, RRID:AB_2082802
Anti-FMN2	Abcam	Cat# ab72052, RRID:AB_1209289
Anti-IREB2	Cell Signaling Technology	Cat# 37135, RRID:AB_2799110
Anti-LRP4	Thermo Fisher Scientific	Cat# PA5-68218, RRID:AB_2691998
Anti-PYGM	Thermo Fisher Scientific	Cat# MA5-27442, RRID:AB_2723538
Anti-UBEK2	Cell Signaling Technology	Cat# 3847, RRID:AB_2210768
Anti-acyl-α -tubulin	Cell Signaling Technologies	Cat# 5335, RRID:AB_10544694
Anti-γ-tubulin	Thermo Fisher Scientific	Cat# PA1-28042, RRID:AB_2256789
Anti-GM130	Novus	Cat# NBP2-53420G, RRID:AB_2890912
Anti-VAMP-7	Abcam	Cat# ab36195, RRID:AB_2212928
Anti-GFP	Thermo Fisher Scientific	Cat# G10362, RRID:AB_2536526
Goat anti-mouse Ig-HRP	BD Biosciences	Cat# 554002, RRID:AB_395198
Goat anti-rabbit Ig-HRP	Thermo Fisher Scientific	Cat# 31460, RRID:AB_228341
Goat anti-rat Ig-HRP	Thermo Fisher Scientific	Cat# 31470, RRID:AB_228356
Bacterial and virus strains		
One Shot™ Stbl3™ Chemically Competent E. coli	Thermo Fisher Scientific	Cat# C737303
Biological samples		
N/A		
Chemicals, peptides, and recombinant proteins		
nocodazole	Millipore Sigma	Cat# M1404; CAS# 31430-18-9
brefeldin A	APExBIO	Cat# B1400; CAS: 20350-15-6
golgicide A	APExBIO	Cat# B1385 ; CAS: 1139889-93-2
mitoNEET Inhibitor NL-1	Millipore Sigma	Cat# 475825
HPA-12	Cayman Chemicals	Cat# 28350 ; CAS 383418-30-2
SMFH2	Millipore Sigma	S4826; CAS 340316-62-3
Cisplatin	Millipore Sigma	Cat# 232120 ; CAS 15663-27-1

REAGENT or RESOURCE	SOURCE	IDENTIFIER
LDLR peptide	Novus	Cat# 06709PEP
CP91149	Selleckchem	Cat# S2717; CAS No. 186392-40-5
NSC-697923		Cat# S7142; CAS No. 343351-67-7
Eltanexor		Cat# S8397; CAS No. 1642300-52-4
Critical commercial assays		
CellLight™ rfp-α-tubulin BacMam 2.0	Thermo Fisher Scientific	Cat# C10503
GeCKOv2 sgRNAs library	Addgene	Cat# 1000000048
Invitrogen™ LIVE/DEAD™ Fixable Far Red Dead Cell Stain Kit, for 633 or 635 nm excitation	Thermo Fisher Scientific	Cat# L10120
SuperSignal™ West Dura Extended Duration Substrate	Thermo Fisher Scientific	Cat# 34075
Deposited data		
A genome-wide hepatocyte CRISPR-CAS9 screen to identify host factors essential for optimal Plasmodium liver stage development.	Mendeley Data	10.17632/75brhkh25r.1
Experimental models: Cell lines		
HepG2-CD81 Human hepatoma cells	Silvie et al., 2006	-
HEK 293-T human kidney cells	Millipore Sigma	Cat# 12022001
Experimental models: Organisms/strains		
P. yoelii wild type strain 17XNL	BEI resources	Cat# MRA-593
Anopheles stephensi mosquitoes	BEI resources	Cat# MRA128
Oligonucleotides (see Table S3 for sgRNA sequences)		
CRISPR/Cas9; All in one lentivector set CENPJ	Applied Biological Materials	Cat# K0432405
CRISPR/Cas9; All in one lentivector set CXCL14	Applied Biological Materials	Cat# K0535905
CRISPR/Cas9; All in one lentivector set FLNA	Applied Biological Materials	Cat# K0787305
CRISPR/Cas9; All in one lentivector set FLT1	Applied Biological Materials	Cat# K0788105
CRISPR/Cas9; All in one lentivector set KDELC1	Applied Biological Materials	Cat# K1128605
CRISPR/Cas9; All in one lentivector set PRPS2	Applied Biological Materials	Cat# K1729505
VPS51 CRISPR/Cas9 KO Plasmid (h)	Santa Cruz Biotechnology	Cat# sc-410709
CRISPR/Cas9; All in one lentivector set XPO1	Applied Biological Materials	Cat# K0006805
CRISPR/Cas9; All in one lentivector set CISD1	Applied Biological Materials	Cat# K0454205
CRISPR/Cas9; All in one lentivector set COL4A3BP	Applied Biological Materials	Cat# K0482705
CRISPR/Cas9; All in one lentivector set FMN2	Applied Biological Materials	Cat# K0789105
CRISPR/Cas9; All in one lentivector set IREB2	Applied Biological Materials	Cat# K1098005
CRISPR/Cas9; All in one lentivector set LRP4	Applied Biological Materials	Cat# K1230305
CRISPR/Cas9; All in one lentivector set PYGM	Applied Biological Materials	Cat# K1764905
CRISPR/Cas9; All in one lentivector set UBEK2	Applied Biological Materials	Cat# K2572605
Software and Algorithms		
Prism version 7	GraphPad Software	graphpad.com
ClueGO	Bindea et al., 2009	http://apps.cytoscape.org/apps/cluego
IMARIS 9.8	Oxford instruments	https://imaris.oxinst.com/
FlowJo	Tree Star	https://www.flowjo.com/

REAGENT or RESOURCE	SOURCE	IDENTIFIER
Huygens Professional Software	Scientific Volume Imaging	https://svi.nl/Huygens-Essential